AD-A189 572 INTERACTION BETWEEN TWO-DIMENSIONAL SONIC JETS AND 1/2
SUPERSONIC FLOW TO MOD (U) AIR FORCE INST OF TECH
WRIGHT-PATTERSON AFB OH SCHOOL OF ENGI J M TRAXLER
UNCLASSIFIED DEC 87 AFIT/GA/AA/87D-07 F/G 21/2 NL

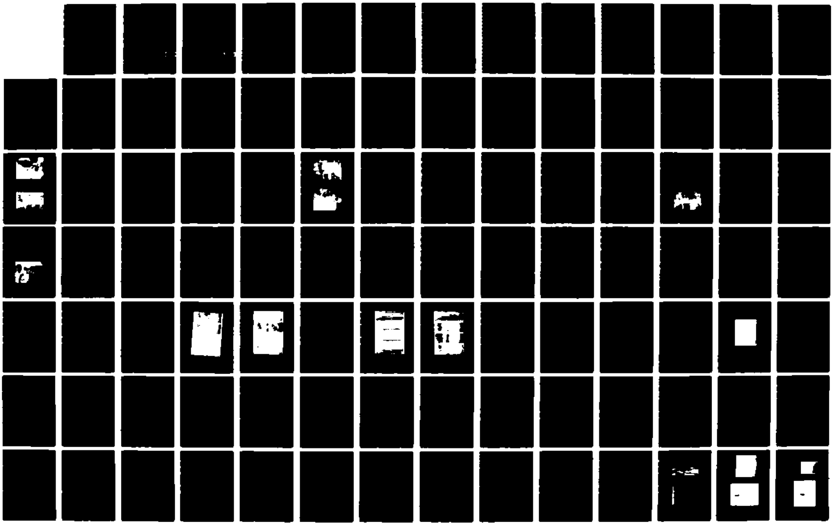

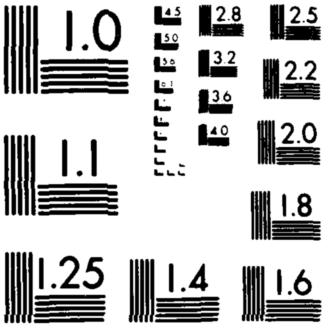
1.0
4.5
5.0
5.6
6.3
2.8
3.2
3.6
4.0
2.5
2.2
2.0
1.1
1.8
1.25
1.4
1.6

MICROCOPY RESOLUTION TEST CHART
NATIONAL BUREAU OF STANDARDS-1963-A

(1)

DTIC FILE COPY

AD-A189 572

INTERACTION BETWEEN TWO-DIMENSIONAL SONIC JETS AND SUPERSONIC FLOW TO MODEL HEAT ADDITION IN A SUPERSONIC COMBUSTOR

THESIS

John M. Traxler
Major, USAF

AFIT/GA/AA/87D-07

DTIC
S MAR 03 1988 D
GH

DEPARTMENT OF THE AIR FORCE
AIR UNIVERSITY
AIR FORCE INSTITUTE OF TECHNOLOGY

Wright-Patterson Air Force Base, Ohio

DISTRIBUTION STATEMENT A
Approved for public release;
Distribution Unlimited

88 3 01 133

(1)

AFIT/GA/AA/87D-07

INTERACTION BETWEEN TWO-DIMENSIONAL SONIC JETS AND SUPERSONIC FLOW TO MODEL HEAT ADDITION IN A SUPERSONIC COMBUSTOR

THESIS

John M. Traxler
Major, USAF

AFIT/GA/AA/87D-07

DTIC
S MAR 03 1988 D

Approved for public release; distribution unlimited

AFIT/GA/AA/87D-07

INTERACTION BETWEEN TWO-DIMENSIONAL SONIC JETS AND SUPERSONIC FLOW TO MODEL HEAT ADDITION IN A SUPERSONIC COMBUSTOR

THESIS

Presented to the Faculty of the School of Engineering
of the Air Force Institute of Technology
Air University
In Partial Fulfillment of the
Requirements for the Degree of
Master of Science in Astronautical Engineering

John M. Traxler, B.S.
Major, USAF

December 1987

Approved for public release; distribution unlimited

Preface

This experimental investigation is a starting point for what I hope is a series of experimental and analytical investigations in the area of heat addition to a supersonic flow.

This report describes my efforts to model supersonic heat addition with mass addition to the supersonic flow provided by an expanding sonic jet. This was followed by a demonstration of supersonic heat addition using an oxy-acetylene torch in a supersonic test cavity.

I wish to acknowledge my sponsor, Dr. Edward T. Curran, Chief Scientist of the Aero Propulsion Laboratory, as the originator and inspiration of this investigation.

I am deeply indebted to my principal faculty advisor, Dr. William C. Elrod, for investing much of his time into this study. He was always willing to teach me experimental techniques by putting his hands to work in the lab, with or ahead of mine.

I wish to thank John Brohas for his excellent work in model fabrication and providing the technical know-how to make an unskilled idea into a properly functioning design.

Of most importance I express my appreciation to my wife, Judy, and children, Amy and Ryan, for their understanding support during my tenure at AFIT.

John M. Traxler

Accession For
NT
D
U
J
Distribution/
Availability Codes
Dist | Avail and/or Special
A-1

DTIC
COPY
INSPECTED
2

*Original contains colour plates: All DTIC reproductions will be in black and white

Table of Contents

Page

Preface ii

List of Figures v

List of Tables viii

List of Symbols ix

Abstract x

I. Introduction 1

  Background 1
  Purpose and Scope 8

II. Experimental Apparatus 10

  Test Section #1 10
  Test Section #2 13
  Test Section #3 15
  Test Section #4 15
  Diffuser 20
  Air Supply 20
  Oxygen-Acetylene Supply 22
  Schlieren System 22
  Instrumentation 23
  Total Pressure Probe 24

III. Experimental Proceedure 25

  Flow Visualization 25
  Pressure Measurements 26
  Heat Addition to Supersonic Flow . . . 27

IV. Theoretical Model 30

V. Results and Discussion 40

  Pressure Measurement Data Reduction . . 40
  Results From Optical Study 44
  Effects of Nozzle Geometry-
    Test Section #1 50
  Test Section #2 55
  Test Section #3 57
  Exit Mach Number 60

Shock Interaction Measurements, Test Sections #2 and #3 63
Other Boundary Layer Effects 67
Momentum Deficit in Wake of Sonic Nozzle 70
Average Flow Conditions In Test Section 75
Test Section #4 - Heat Addition by Combustion 79

VI. Conclusions and Recommendations 86

Conclusions 86
Recommendations 87

Bibliography 89

Appendix A: Selected Data Sets For Test Sections #1-#3 92

Vita 98

List of Figures

Figure Page

1. Schematic of Hypersonic Dual Combustion Ramjet (4:417) 6

2. Shock Expansion and Combustion Zones in Supersonic Combustor (4:420) 6

3. Schematic of Test Section #2 12

4. Picture of Test Section #1 Attached to Stilling Chambers and Diffuser 14

5. Picture of Test Section #2 with Pressure Measurement Sidewall 14

6. Schematic of Test Section #4 17

7. Picture of Test Section #4 with Quartz Windows in a Metal Frame 19

8. Picture of Test Section #4 with Short Plexiglass Sidewalls 19

9. Schematics of Air Supply 21

10. Picture of Test Section #2 with Tygon Tubing Attached 25

11. Igniting Test Section #4 28

12. Base Bleed Model 31

13. Expanding Flow Model 34

14. Theoretical Mach Number for Secondary and Primary Streams vs. Reservoir Pressure Ratio for Geometry of Test Sections #2 and #3 38

15. Theoretical Primary Flow Normalized Pressure and Mass Flux Ratio for Test Section #2 and #3 38

16. Upper Primary Nozzle Centerline Pressures, Showing Diffusion Through Boundary Layer . 43

17. Composite Schlieren Photographs of Flow in Test Section #1 with Primary/Secondary Reservoir Pressure of:
(a) 75 psig / 50 psig (b) 84 psig /22 psig
(c) 84 psig / 10 psig (d) 84 psig /0 psig 45

18. Composite Schlieren Photographs of Flow in Test Section #2 with Knife Edge Perpendicular to Flow Direction with Primary/Secondary Reservoir Pressure of:
(a) 85 psig / 10 psig (b) 84 psig /20 psig
(c) 83 psig / 30 psig (d) 82 psig /40 psig 46
(e) Nomenclature for Photograph Description 47

19. Composite Schlieren Photographs of Flow in Test Section #2 with Knife Edge Parallel to Flow with Knife Edge Parallel to Flow with Primary/Secondary Reservoir Presure of:
(a) 87 psig / 0 psig (b) 85 psig /10 psig
(c) 84 psig / 22 psig (d) 79 psig /58 psig 48

20. Composite Schlieren Photographs of Flow in Test Section #3, Knife Edge Parallel in (a) only, with Primary/Secondary Reservoir Pressure of:
(a) 67 psig / 32 psig (b) 67 psig /32 psig
(c) 69 psig / 15 psig (d) 70 psig /10 psig 49

21. Off-Design Nozzle Configuration 51

22. Schlieren Photograph of the Nozzle Area of Test Section #1 54

23. Test Section #3 Nozzle Centerline Static Pressure 59

24. Nozzle Exit Static Pressures for Test Sections #2 and #3 Compared with Isentropic 62

25. Measured Base Pressures, Compared with One Dimensional Theory 64

26. Interaction Shock Angles for Test Sections #2 and #3 65

27. Test Section #2 Upper Centerline Static Pressures 68

28. Test Section #3 Upper Centerline Static Pressures 68

29. Comparison of Static Pressure in Test Sections #2 and #3 for the Same Secondary-to-Primary Reservoir Pressure Ratio. . . . 69

30. Similarity of Static Pressure at Same Reservoir Pressure Ratio Adjusted for Total Pressure Difference 71

31. Nozzle Centerline Mach Number with Weaker Shock, Measured in Test Section #3 vs. Adjusted Theoretical 73

32. Nozzle Centerline Mach Number with Stronger Shock, Measured in Test Section #3 vs. Adjusted Theoretical 73

33. Average Static Pressures for Test Section #3 76

34. Average Total Pressures for Test Section #3 77

35. Average Mach Number for Test Section #3 . 78

36. Cold Flow in Test Section #4 with Long Plexiglass Sidewall 81

37. Cold Flow in Test Section #4 with Short Plexiglass Sidewall, Same Length as Combustion Model 81

38. Flow in Free Area Beyond Windows with No Flame Test Section #4 82

39. Picture of Flame in Test Section #4 with No Air Flow 82

40. Schlieren of Test Section #4 with Combustion Heat Addition 83

41. Picture of Oxygen-Rich Flame in Test Section #4 83

42. Schematic of Flow in Test Section #4 with Heat Addition 85

List of Tables

Table Page

1. One Dimensional Analysis of Test Sections #2 and #3 as Designed 37

2. One Dimensional Analysis of Test Section #3 for Exit Mach Number = 2.8 74

3. Comparison of Friction and Oblique Shocks. to Cause Measured Properties 79

4. Data Set, Test Section #1 93

5. Data Set, Test Section #2 94

6. Data Set, Test Section #3 95

7. Data Set, Test Section #1 at Highest Secondary-to-Primary Reservoir Ratio Tested 96

8. Data Set, Test Section #2 at Highest Secondary-to-Primary Reservoir Ratio Tested 97

List of Symbols

A	Nondimensional mass addition quantity, or Cross Sectional Area
A^*	Cross-sectional area at Mach number unity
B	Nondimensional momentum addition quantity
C	Nondimensional heat addition quantity
MFR	Mass Flux Ratio
P_b	Base pressure
Po	Reservoir pressure
Po_s	Secondary reservoir presssure
Po_p	Primary Reservoir pressure
Po_x	Total Pressure Upstream of Shock
Po_y	Total Pressure Downstream of Shock
P_x	Static Pressure Upstream of Shock

AFIT/GA/AA/87D-07

Abstract

The displacement effects of heat addition to a supersonic flow through a simulated combustor were simulated with mass addition.

The structure of precombustion shocks was experimentally investigated by an optical and pressure study of two parallel sonic jets expanding into a two-dimensional supersonic test cavity. Base flow and recompression shocks were studied for two test section depths. A test section to add heat to a two dimensional flow was demonstrated.

It was determined that the performance of the constant-area test section was dominated by frictional, rather than shock effects. An off-design nozzle was used for preliminary investigation and caused turbulence and high losses in the channel.

The structure of the precombustion zone was found to be a base flow problem and was analyzed using a simple one dimensional model.

Static pressure measurements on the sidewalls of the test cavity were found to differ from the static pressure in the center of the two dimensional test cavity, due to diffusion of pressure upstream and downstream through the boundary layer.

A welding torch was used to inject premixed oxygen and acetylene into the base region on the end of a centerbody between two supersonic nozzles. The flame was sucessfully ignited and burned continuously in the flowstream. However, the large amount of heat added caused flow separation in the supersonic nozzles.

INTERACTION BETWEEN UNDEREXPANDED TWO-DIMENSIONAL SONIC JETS AND TWO-DIMENSIONAL SUPERSONIC FLOW TO MODEL HEAT ADDITION IN SUPERSONIC FLOW

I. Introduction

The hypersonic airbreathing engine is the subject of a major research and development effort today. A subsonic combustion ramjet would have extremely high static temperatures and pressures at hypersonic speeds. At a flight Mach number of 12, temperature would actually decrease in a subsonic combustor as hydrogen fuel is added (13:33), due to dissociation. Heating of the propellant gases would occur in the nozzle as the flow expands and some of the molecules recombine from the dissociated state established in the combustor. Since this process is not instantaneous, large frozen flow losses would occur. The hypersonic ramjet cycle is much more efficient if fuel is injected in the air where the flow is supersonic and the temperature is low enough to allow complete reaction to occur.

Background

The design of an efficient supersonic combustion ramjet (SCRAMJET) requires the designer be able to control the geometry- and combustion-induced shocks in the inlet and combustor. Shocks in supersonic combustors are generated by a variety of sources, including (15:2):

a. reflected and incident inlet shocks,

b. flow separation regions,

c. fuel injection, and injection struts,

d. film cooling injection,

e. interference shocks from corners and intersecting shocks.

Normally, strong shocks are avoided in supersonic combustor design. Strong shocks may be formed in a duct when heat is released too rapidly. Thermal choking for a constant-area combustor occurs when exit velocity is reduced to sonic speed. This limits the amount of heat that may be added to a supersonic flow. Adding more heat to a thermally-choked flow will cause a shock wave to form upstream and unstart the combustor (25:51). Obviously, a higher Mach number at the combustor entrance allows more heat to be released in the supersonic flow.

Billig suggests (6:1129) that a shock wave in a combustor does not always result in reduced cycle efficiency. The shock total pressure loss may be compensated by reduction of total pressure loss due to burning at a lower Mach number. He found that the most efficient combustor had the lowest static pressure increase for a given amount of heat addition.

Mixing rate normally limits the supersonic combustion process (25:48), except in the upstream portion, which is certainly controlled by chemical reaction kinetics. Rapid mixing and fast chemical reactions are required to keep the combustor from becoming excessively long. Mixing is greatly reduced in supersonic flows and decreases as Mach number increases. Kumar found by numerical analysis (15) that an oscillating shock would enhance turbulence, and hence, mixing in a supersonic stream. A typical scramjet uses gaseous fuel injection, both parallel and perpendicular to the primary flow (28:1426). Perpendicular fuel injection causes rapid mixing to allow reaction in the upstream portion of the combustor. The injected stream separates the boundary layer, which causes a bow shock in front of the injector and turns the primary flow away from the injector. A subsonic separation and recirculation region, caused by rapid expansion of the fuel jet, acts as a flameholder. At low Mach numbers, in the M=4-5 range, parallel injection is used to slow the mixing process and prevent thermal choking. Experiments done by Bonney (7), and Carlile (8) on two-dimensional air and helium supersonic mixing, which served as a basis for this study, determined that mixing occurs at a very slow rate, even with a large difference in density.

A perpendicular injector or a fuel strut produces a momentum deficit downstream, often with regions of flow expansion and recompression. This becomes a primary mixing mechanism (27). The flow pattern in such a combustor resembles a supersonic wake region with base injection. Base flows and wakes have been well studied and a number of base flow models developed, such as that by Korst (14). Chow's analysis (10), based on Korst theory, of base flow due to interaction between two-dimensional sonic jets and supersonic flow has direct application to this study.

Combustor length can be reduced by fuel injectors in the inlet system (25:50). Billig's analysis (2) suggested using combustion in one of two inlet streams to compress the other. "Thermal compression" could be used in lieu of variable geometry in changing flow conditions. "Thermal compression" (5, 1:10-11) would replace some of the oblique shocks in a supersonic inlet with an infinitesimally thin flame front called an oblique planar heater (OPH) which adds heat and changes the velocity vector of the flow. "Thermal compression" gains in performance are greatest at low flight Mach number and small contraction ratios. For example, a fixed-geometry engine with a contraction ratio of 4, can increase specific inpulse 61% at Mach 5 by using "thermal compression." The increase is only 3.5% at Mach 12 with a contraction ratio of 10. A properly designed fuel injection system will save fuel during acceleration to hypersonic speeds.

Oblique shocks may be desirable in a combustor to stabilize the flame front. Experiments have shown (6:1136) the position of a shock-stabilized flame front is nearly independent of both fuel mass flow rate and temperature over a wide range of temperatures. The oblique shock significantly reduced the ignition-delay distance.

The concept of a Hypersonic Dual Combustion Ramjet requires mixing of sonic and supersonic jets in the combustion process (1:2). This configuration is seen in Figure 1. Most of the inlet air bypasses the subsonic combustor through a duct to a supersonic combustor. All fuel is added in the subsonic combustor. The hot fuel-rich sonic jet from the subsonic combustor expands into the supersonic combustor producing precombustion shocks (4:420). The shock-expansion zone is followed by a highly two-or three-dimensional combustion zone, as seen in Figure 2. The mixing and heat release cause pressure disturbances which produce shocks upstream in the supersonic duct through the boundary layer and base flow region. As more heat is added the shocks in the precombustion zone become stronger. The stronger shock may increase mixing, which would cause more heat release, if the combustion is controlled by mixing. A sufficiently mixed flow may even be ignited by a strong shock that raises the static temperature to the ignition point (19).

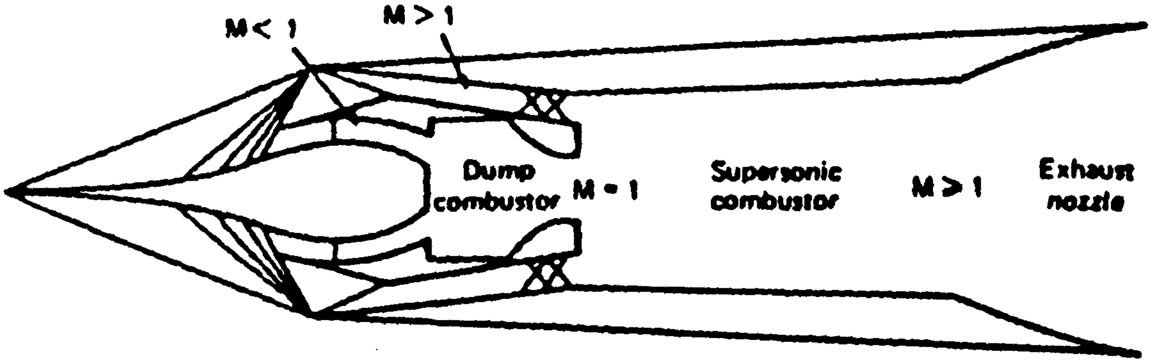
M< 1
M > 1
Dump combustor
M = 1
Supersonic combustor
M > 1
Exhaust nozzle

Dual mode ramjet configuration

Figure 1. Schematic of Hypersonic Dual Combustion Ramjet (4:417)

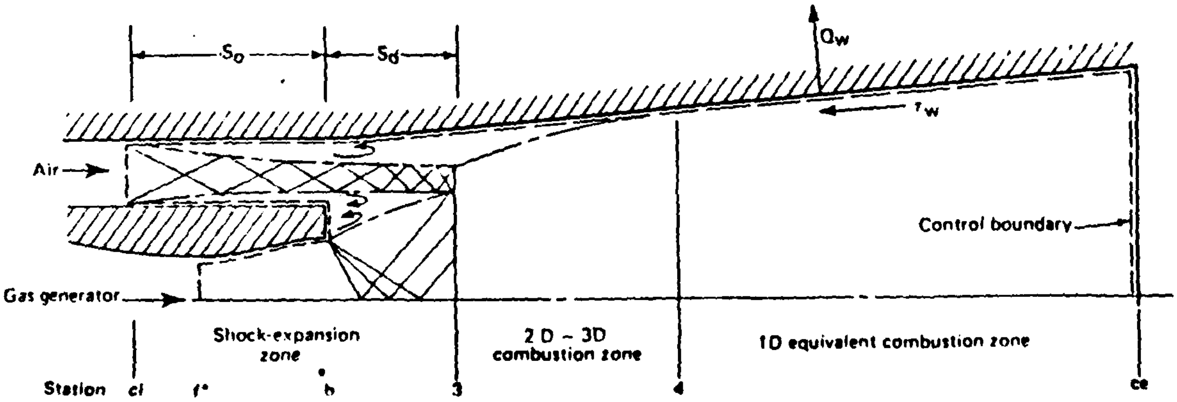
S_0
S_d
Q_w
τ_w
Air
Control boundary
Gas generator
Shock-expansion zone
2 D ~ 3D combustion zone
1D equivalent combustion zone
Station
ci
f*
b
3
4
ce

Figure 2. Shock Expansion and Combusion Zones in Supersonic Combustor (4:420)

Spier's analysis (24) emphasized the importance of properly predicting the rate of mixing and burning to prevent thermal choking, especially in combustors with small expansion ratios. The rate at which sonic fuel and supersonic air streams mix and exchange momentum determines the Mach number at each location for each stream. This determines how much heat can be added to the partially mixed stream before thermal choking occurs.

Rues investigated (18) a basic equivalence between mass-, force-, and energy-sources. He solved the integral equations of the conservation laws for two-dimensional subsonic flow. The two-dimensional supersonic solution exists, but is not presented. His analysis shed light on a previous observation "that adding energy to a flow has a displacement effect, similar to that of a mass-source (18:3)."

Zierep's one dimensional analysis (29:10-12) reveals that the similarity parameter, S, between heat-, mass-, and momentum-addition has the form:

$$S = (1+C)(1+A)^2/(1+B)^2$$

where A, B, and C are non-dimensional quantities for addition of mass, momentum, and heat respectively. Different choices of A and C will obviously result in the same value of S. However, Zierep warns "we cannot expect that the equivalence extends so far that a particular mass addition can be in all respects replaced by a certain energy addition - that is, that all the flow quantities thereby remain unchanged (29:12)."

Purpose and Scope

Basic research in supersonic combustion is far from complete, and the subject is broad and complex. This study concentrates on only a small area of the supersonic combustion problem. The purpose of this study is to get away from the technology of burning and look only at the gas dynamics of heat addition to a supersonic flow, such as shock structure, and some indicators of mixing rates, with increasing amounts of heat release.

The analogy between heat- and mass-addition inspired a major portion of this study. The displacement effect of heat addition was replaced with an expanding sonic jet. This models a zone of combustion displacement in "thermal compression" or the shock expansion zone of the Hypersonic Dual Combustion Ramjet.

This investigation had three major objectives:

1. Determine the structure of flow, shocks, and some indicators of mixing, in the pre-combustion shock expansion region of a supersonic combustor by simulating heat addition with mass addition.
2. Determine the possibility of compressing a supersonic stream with an expanding sonic jet to simulate heat addition.

3. Design a test section for later investigation on the effects of combustion heat addition in a supersonic flow.

The first objective was accomplished by an experimental investigation that included schlieren flow visualization, and static and total pressure measurements, of flow from two parallel sonic jets spreading into the surrounding supersonic flow with two test section depths and several pressure ratios.

The second objective was completed theoretically by developing a one dimensional model of the expanding flow, and experimentally by measuring sidewall static pressures on the centerline of one of the supersonic nozzles.

The third objective was completed by demonstrating combustion of premixed oxygen and acetylene in the wake region between two supersonic nozzles.

No attempt was made to measure pressures or temperatures in the combustion model. The analogy between heat and mass addition was not used quantitatively to compare the cold-flow investigation to a particular, equivalent hot-flow condition.

II. Experimental Apparatus

The experimental equipment included four test sections, a diffuser with a traversing mechanism for holding a total pressure probe, an air supply, an oxygen-acetylene supply for the combustion tests, a schlieren system, and instrumentation.

Test Section #1

The first test section was a modification of one designed by Captain John D. Carlile (8) to study supersonic air-helium mixing. Test sections #2 and #3 were further modifications of this design. The supersonic helium nozzles of Carlile's design were replaced with sonic air nozzles. The sonic nozzles were designed with the nozzle throat at the nozzle exit plane so that the air leaving the nozzle would be at sonic velocity. The test section was made of plexiglass sidewalls 10.5 inches long, 4.4 inches wide, enclosing a test cavity 2.375 inches wide and .375 inches deep. The first inch of the cavity was a subsonic approach to the nozzle assembly.

The nozzle assembly consisted of three supersonic air nozzles sandwiching two sonic sharp corner nozzles. The sonic nozzles were in the center of two aluminum nozzle blocks which, along with two half nozzles, formed the three supersonic air nozzles. The configuration of the nozzle assembly is the same for test sections #1-#3. It is shown in Figure 3, with dimensions of test section #2.

For all flow conditions investigated with test section #1-#3, more mass flowed through the supersonic nozzles than through the sonic nozzles. Therefore, the supersonic nozzles, and flow through them, are later referred to as primary. The sonic nozzles, and their flow, are referred to as secondary.

The air for the sonic nozzles entered both sides of a .375 inch diameter cylindrical chamber in each nozzle block through fittings in both sidewalls. The four fittings were connected to 3/8 inch outside diameter copper tubing, which supplied air from a secondary stilling chamber. The air approached the .102 by .375 inch throat through a .195 by .375 inch rectangular duct. The throat was designed to produce a sonic jet which would expand into the surrounding supersonic flow. The height of the sonic nozzle block at its end was .312 inches.

The supersonic air nozzles were designed by method-of-characteristics to accelerate air to Mach 3 through a .133 by .375 inch sharp-corner throat and .563 by .375 inch exit. The nozzle blocks were manufactured according to the same specifications as the original nozzle blocks used by Carlile, However, when placed in the test section, the throat dimensions were actually .109, .112, .109 by

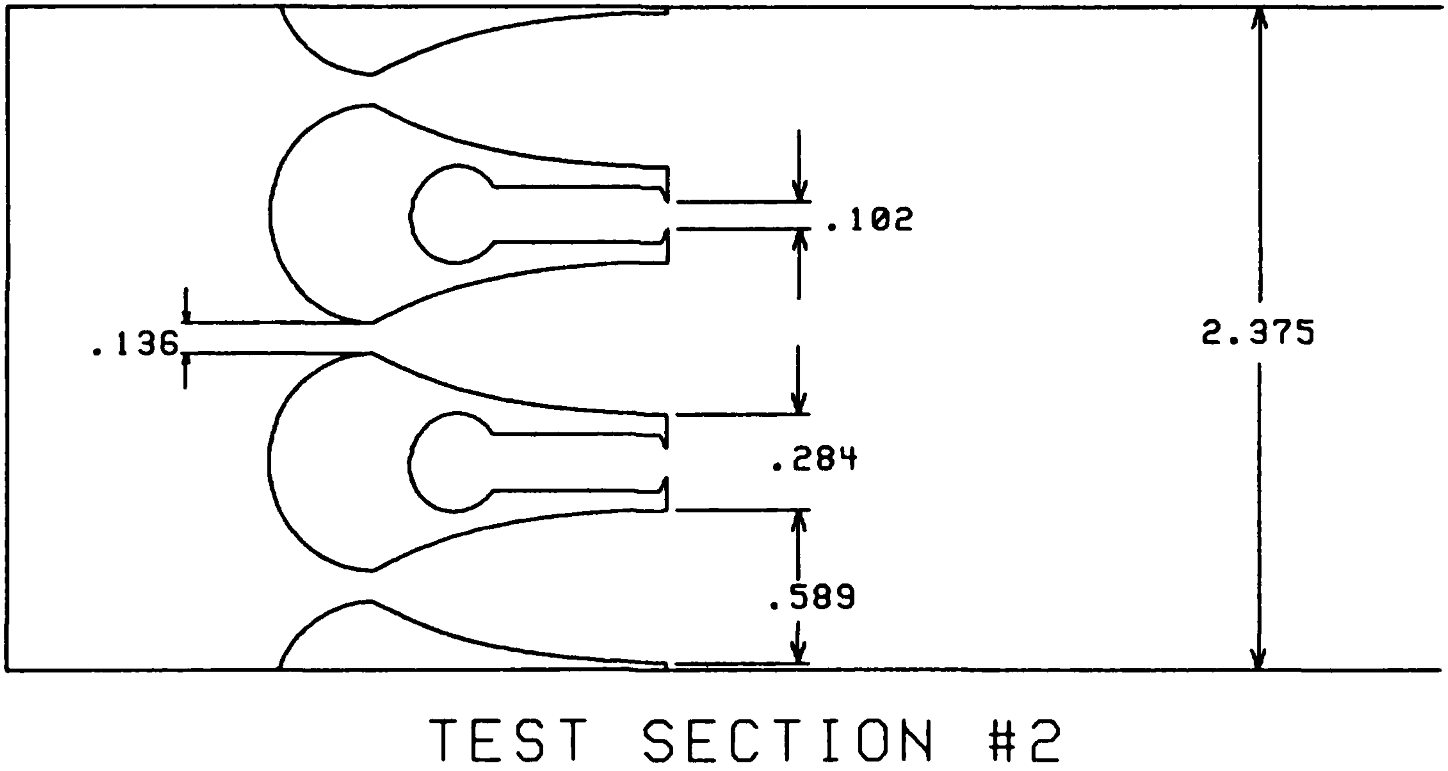
.102
.136
.284
.589
2.375
TEST SECTION #2

Figure 3. Schematic of Test Section #2

.375 inches for the upper, center, and lower nozzles respectively. The exit dimensions measured .561 by .375 inches. These nozzles were used in this off-design configuration for the preliminary investigation.

The supersonic test cavity was over 7 inches long. One permanent sidewall was equipped with static pressure taps at the exit plane of all five nozzles. The other sidewall was interchangeable, a clear sidewall for schlieren photography, or a sidewall with five rows of nine pressure taps. The first row was .750 inches from the nozzle exit plane followed by four rows spaced one inch apart. The first, fifth, and ninth pressure taps were on the centerline of the supersonic nozzles. The third and seventh on the centerline of the sonic nozzles.

An aluminum plate on the upstream end of the test cavity attached to the stilling chamber. A plate on the downstream end attached to the variable diffuser. The test equipment is shown assembled in Figure 4.

Test Section #2

The second test section was like the first, except the nozzle blocks were remanufactured to produce a .136 inch throat and .589 inch exit. This provided an area ratio to accelerate the air to Mach 3.02. The height of the sonic nozzle block at its end was .284 inches. The sidewalls were replaced with two clear sidewalls for schlieren photography and one sidewall, shown in Figure 5,

Figure 4. Picture of Test Section #1 Attached to Stilling Chambers and Diffuser

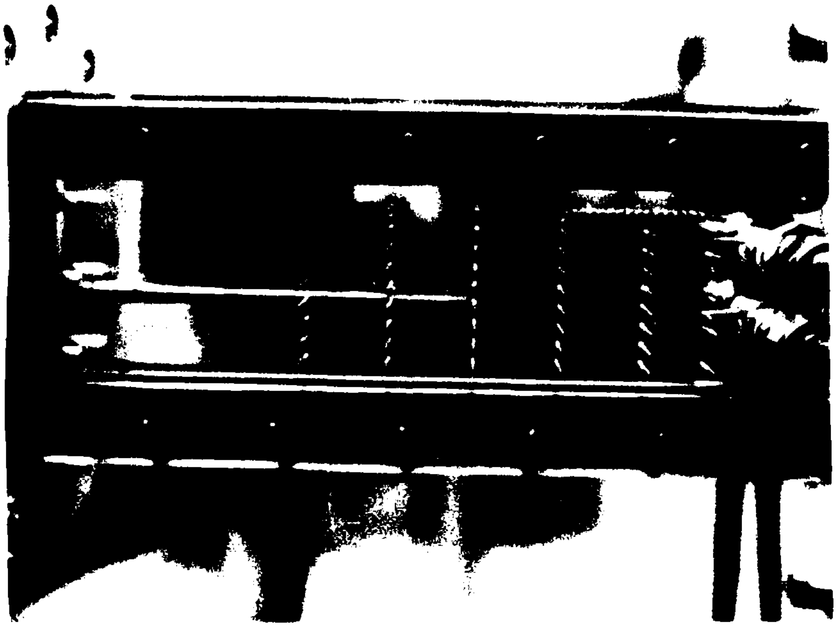

Figure 5. Picture of Test Section #2 with Pressure Measurement Sidewall

with all pressure taps. The pressure taps were in the same location, with added taps on the centerline of the upper supersonic nozzle every .107 inch from the exit plane of the upper supersonic nozzle to the row at 1.750 inches from the exit plane.

Test Section #3

The third test section was made with some interchangeable parts from the second. The nozzle blocks, and upper and lower sidewalls were replaced to make the test cavity .625 inches deep. All other dimensions remained the same, except the upper nozzle throat measured .138 instead of .133. This created a Mach 3.00 rather than Mach 3.04 area ratio.

Test Section #4

The fourth test section was designed to add heat, by combustion, to supersonic flow. Creating a heat addition source by combustion in a low enthalpy flow was expected to be problematic. Injection of a premixed fuel and oxygen into a base flow region was thought to be a solution to this problem. Acetylene was chosen as the primary fuel because of its relatively low spontaneous ignition temperature, 581 degrees Farenheit, and high heating value, 20,790 BTU/lb fuel (3:4). The design is also capable of hydrogen combustion with little modification, but is beyond the scope of this investigation.

The test section, as shown in Figure 6, had a centerbody that formed half of two Mach 3.02 method-of-characteristics nozzles with a sharp corner throat. The centerbody ended with an abrupt step. The blunt end created a recirculation region and wake which acted as a bluff body flame stabilizer.

The test cavity measured .750 inches deep. The heat was produced by an oxygen-acetylene welding torch. A Smith 209 tip was modified to fit into the centerbody. The centerbody measured .625 inches upstream of the throat. The upstream nozzle contour was a one inch radius to the sharp corner throat. The upper and lower nozzle throats measured .201 and .199 inches, with exits of .866 and .859 inches, respectively. This matched the area ratios of the two nozzles at 4.31.

The centerbody ended at the nozzle exit plane five inches from the beginning of the test cavity. The distance between the two nozzles, across the end was .4 inches. This made the width of the test cavity 2.125 inches. A .072 diameter tube injected the premixed oxygen-acetylene into the wake region behind the end of the centerbody.

The upper and lower walls were made of aluminum 13.5 inches long, 1.0 inch wide, and .75 inches thick. The sidewalls over the nozzle section were aluminum plates 5 inches long, 4 inches wide, and .5 inches thick.

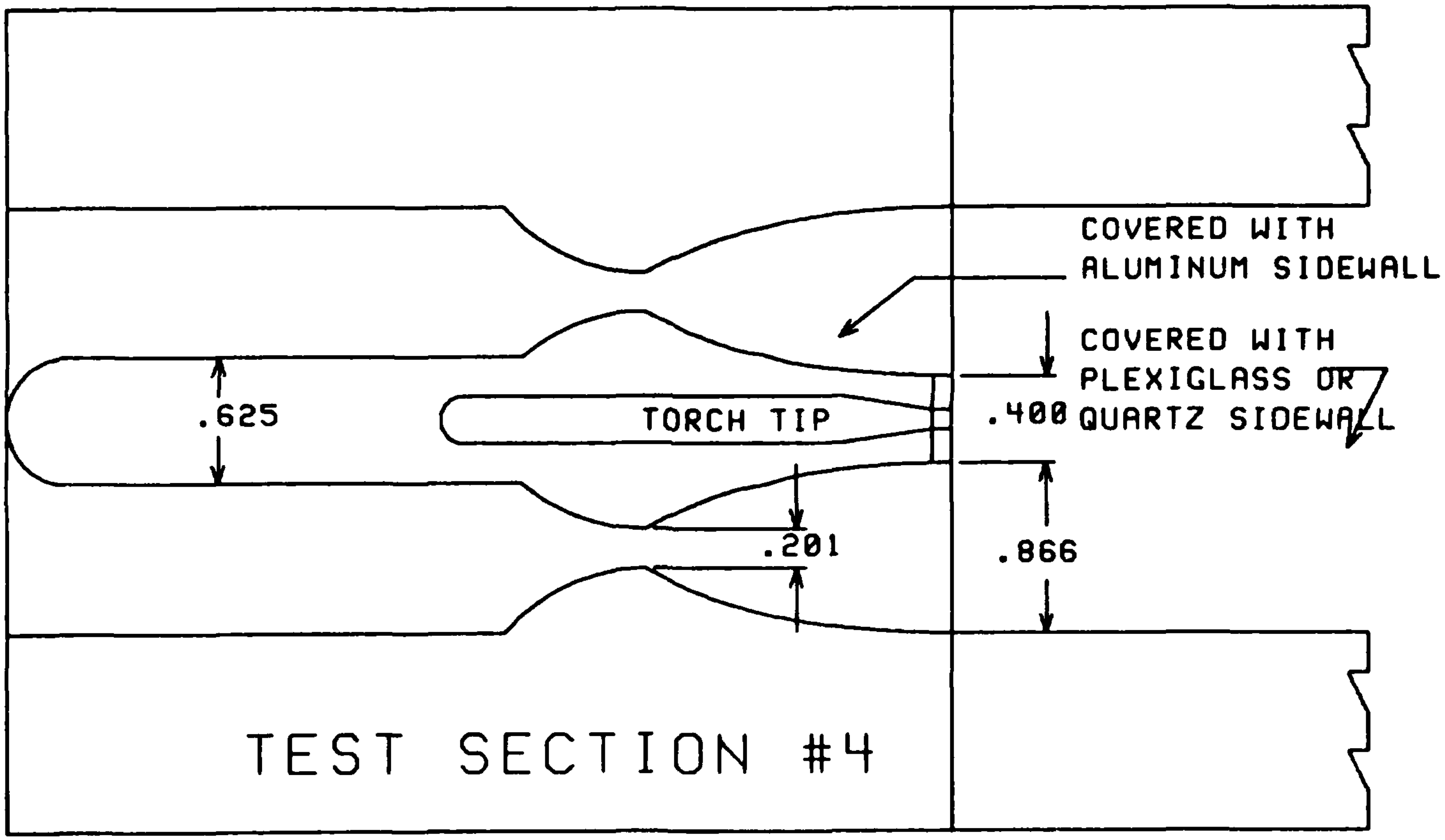
COVERED WITH
ALUMINUM SIDEWALL
COVERED WITH
PLEXIGLASS OR
QUARTZ SIDEWALL
.400
.625
TORCH TIP
.201
.866
TEST SECTION #4

Figure 6. Schematic of Test Section #4

Plexiglass sidewalls enclosed the test cavity for cold flow tests. A set of clear sidewalls measuring 8.5 inches long, 4 inches wide, and .75 inches thick was used for schlieren photography.

One sidewall was changed for making static pressure measurements. It had six rows of seven pressure taps, one tap at each of the two nozzle exits and one in the wake region. The first row was .750 inches from the nozzle exit plane and succeeding rows spaced at one inch intervals. The second and sixth pressure taps on each row were on the nozzle centerline. The fourth tap was on the centerline of the wake behind the end of the centerbody with other taps equally spaced between. An aluminum plate was attached to the end of the plexiglass sidewalls to serve as a mounting plate for the diffuser.

For flow with combustion, sidewalls were made of clear fused quartz measuring 3.250 inches wide, 2.0 inches long, and .375 inches thick. The quartz was mounted in a frame which attached to the upper and lower wall. The frame covered .375 inches of the quartz and extended .750 inches beyond the quartz. This is pictured in Figure 7. A set of clear plexiglass sidewalls 2.75 inches long, was used for cold flow schlieren photography of the area blocked by the frame. This configuration is pictured in Figure 8.

Figure 7. Picture of Test Section #4 with Quartz Windows in a Metal Frame

Figure 8. Picture of Test Section #4 with Short Plexiglass Sidewalls

Diffuser

A five-inch long variable diffuser was mounted to the end of the test cavity. The diffuser was designed to stabilize the flow exhausting to atmosphere. Three sets of ramps .375, .625, and .750 inches wide were interchangeable to use with the corresponding test section. The exit dimension could be adjusted with a screw mechanism from zero to 2.625 inches.

A bracket to hold a .250 inch diameter total pressure probe was mounted on the end of the diffuser. It can be seen in Figure 4. The probe could traverse the width of the test cavity from top-to-bottom by turning a screw mechanism by hand.

Air Supply

Air from facility compressors was supplied to the test equipment at 100 psig through a three-inch supply line. An orifice with .750 diameter bore restricted flow in the supply line. It was replaced for later tests with one of 1.50 inch diameter bore. As depicted in Figure 9, the air passed through a centrifugal separator to remove water and dust before passing through a filter. A "T" in the line separated the primary air supply from the secondary.

The primary air passed through a stilling chamber enroute to the test section. The primary stilling chamber was a cylinder of ten inches inside diameter and over six

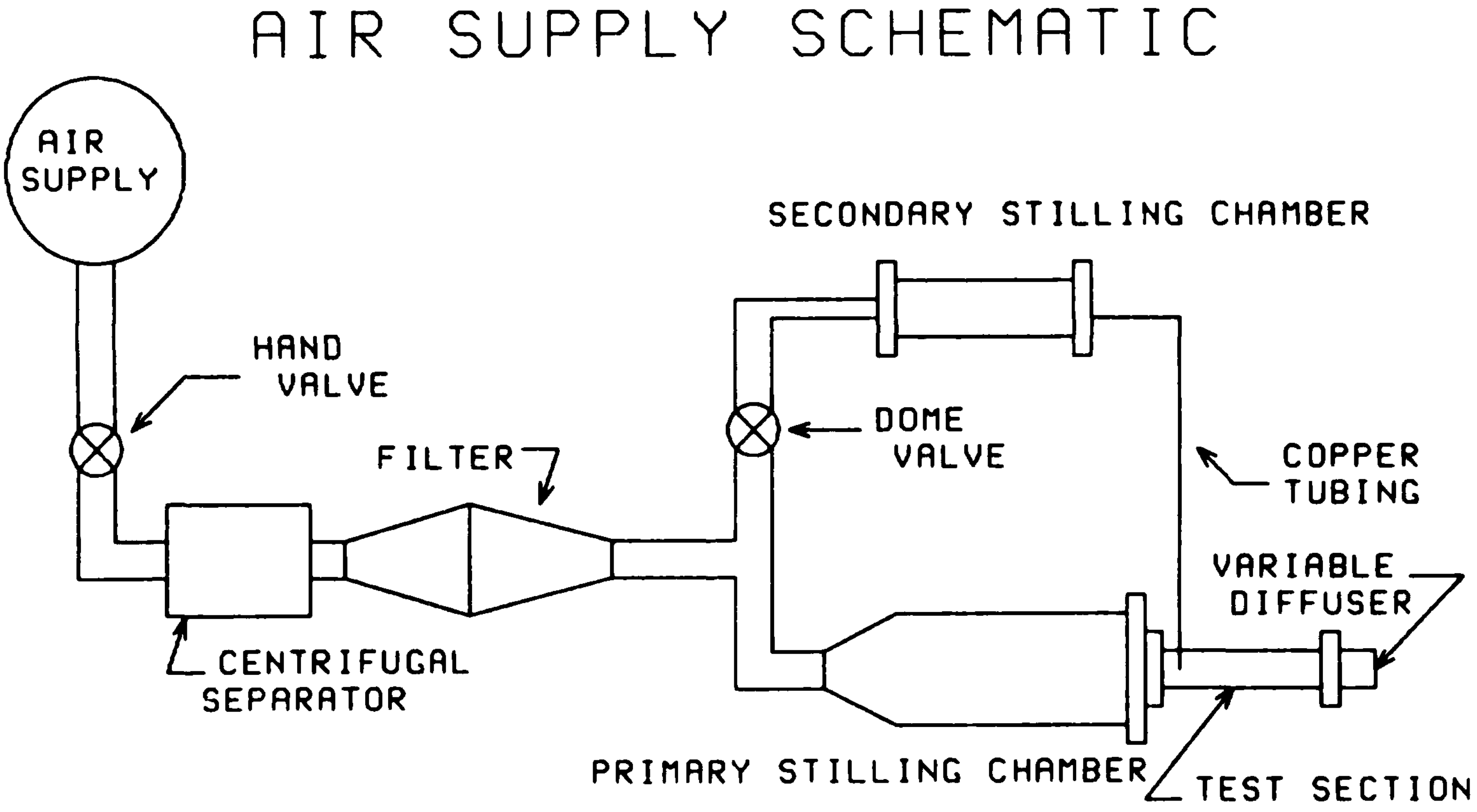
AIR SUPPLY SCHEMATIC
AIR SUPPLY
HAND VALVE
FILTER
CENTRIFUGAL SEPARATOR
SECONDARY STILLING CHAMBER
DOME VALVE
COPPER TUBING
VARIABLE DIFFUSER
PRIMARY STILLING CHAMBER
TEST SECTION

Figure 9. Schematic of Air Supply

feet long. Baffles and a paper filter assembly inside the chamber served to remove turbulence and solid particles from the air.

Secondary air pressure was supplied to test sections #1-#3. It was regulated by a dome valve controlled by a Grove regulator. The secondary stilling chamber was galvanized pipe, seven feet long, with an inside diameter of 2.125 inches. The secondary air was fed to the test section through four copper tubes with inside diameter of .275 inches.

Oxygen-Acetylene Supply

Oxygen and acetylene were supplied to test section #4 through regulators, and a 25-foot double hose. Flow was controlled by valves on the welding torch handle supplied with the welding kit.

Schlieren System

A schlieren system was used to view the flow in all test sections. The system used two 30-inch focal length mirrors. Real time viewing was possible using a steady zirconium arc lamp and frosted glass placed at the focal plane. A Cordin model 5401 spark lamp was used for Polaroid photography. Most pictures were taken with Polaroid Type 42, ASA 200, roll film. Pictures of the combustion model used Type 55, ASA 50, black-and-white and Type 58, ASA 75, color film in the 4" x 5" format.

Instrumentation

The pressures in the primary and secondary stilling chambers were measured using 0-160 psig dial gages calibrated to ±1.0 psi. Atmospheric pressure readings were taken from the digital readout on a standard vacuum source, which was also used as reference for calibration of all pressure measuring devices.

Static and total pressures were measured by a Druck PDCR 22 pressure transducer, through a Scanivalve. The transducer had a 25 psi rated range, however the output was still linear 70% above the rated range. Each pressure port was connected to the Scanivalve by 24 inches of Tygon tubing. The total pressure probe, when in use, was connected to the Scanivalve home position. The signal to step the Scanivalve solinoid was generated by a digital-to-analog converter within a Zenith 100 computer. The 12-volt power supply provided the required potential across the transducer. The output was measured by a analog-to-digital converter in the computer. The gain of the converter was 20 mv which produced a resolution of .00488 mv. Noise in the system averaged approximately ±.03 mv and was no more than ±.2 mv. The error due to noise averaged .01 psi, and was no greater than .07 psi.

Total Pressure Probe

The total pressure probe was a .250-inch diameter stainless steel tube 18 inches long tapered to a .060 inch diameter pitot tube tip 1.5 inches long. Tygon tube connected a .060 inch outlet tube to the Scanivalve.

III. Experimental Proceedure

This experimental investigation was divided into three areas: (1) flow visualization by schlieren photography, (2) static and total pressure measurements, and (3) heat addition to supersonic flow.

Flow Visualization

The large number of tygon tubes required for pressure measurement obscured the flowfield, as pictured in Figure 10. Therefore, schlieren photographs were taken with the clear sidewall in place, before pressures were measured.

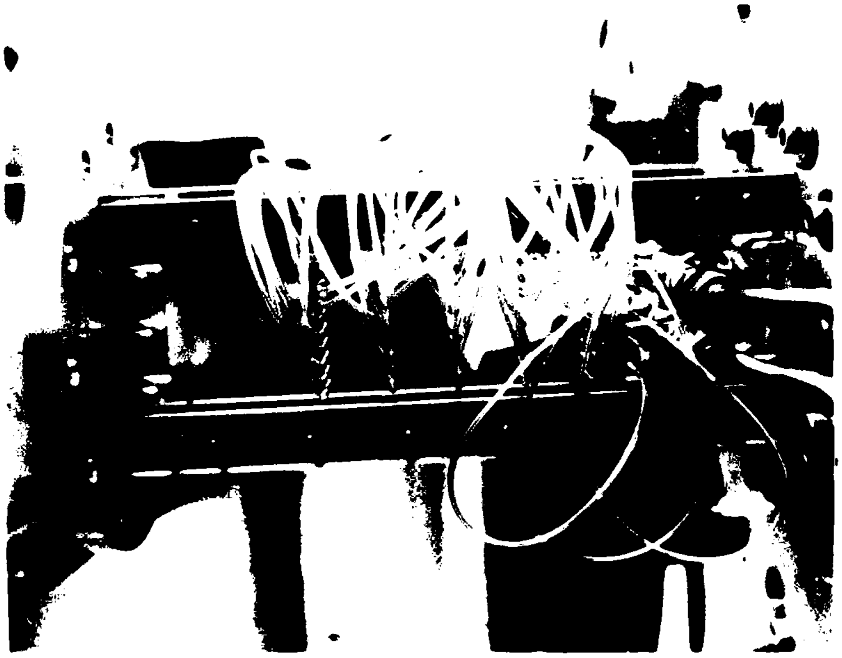

Figure 10. Picture of Test Section #2 with Tygon Tubing Attached

At least two consecutive photos were taken to ensure the conditions were steady state, not transient. The knife edge was positioned both parallel and perpendicular to the flow during the photographic investigation. Original photographs of test section #1 were 58% and 122% actual size. Photographs of test sections #2-#4 were taken 56% of actual size. The entire flowfield can be seen in the smaller scale photographs. Photos were also made with pressure taps covered, when that sidewall was in place, to aid in correlating pressure data with a flow region.

Pressure Measurements

Pressure was measured automatically by computer. Each pressure was measured 20 times and the result was averaged to reduce noise effects. The 48-port cycle required 75 seconds to complete. At high mass flow rates, a slight decrease in source pressure was observed during this cycle. This is a possible source of error.

Static pressures and pitot pressures were not measured simultaneously. After static pressure measurements were complete, the total pressure probe was connected to the home station of the scanivalve and inserted into the center of the test cavity through the retaining bracket. The diffuser was opened to compensate for exit area blocked by the probe. The probe was manually positioned over each pressure tap location in the center of the test cavity with the traversing mechanism.

The computer measured pitot pressure when manually prompted after the probe was in place. Base pressures were also measured by placing the pitot probe within a few thousandths of the solid boundary of the centerbody step. After pitot pressure was measured at each tap, the probe was removed and static pressures were again measured.

Source pressure was constant for all flow conditions for test sections #1 and #2. Pitot pressures were measured with no interuption. The average time required was about 15 minutes. A drop in source pressure, due to high mass flow rates with test sections #3 and #4, required interuption of air flow between measurements of each row. This allowed pitot pressure measurements at nearly the same source pressure as for the static pressure measurements. Caution ensured the same flow condition existed when flow resumed.

Heat Addition to Supersonic Flow

Pressure measurements, for 45 taps, and schlieren photographs were made as above on test section #4 with the 8.5 inch long sidewalls installed. Schlieren photographs were also made with the 2.75 inch clear plexiglass sidewalls. During these tests compressed air, instead of the oxygen-acetylene mixture, was injected into the base region through the torch tip to prevent the accumulation of combustible gases in the room and possible explosion. The molecular weight of acetylene is near that of air.

Combustion was successfully accomplished by the following procedure:

(1) Allow a small amount of primary air to flow to provide cooling.

(2) Open valves on the torch handle to begin fuel flow.

(3) Ignite the flame using a standard torch igniter, as seen in Figure 11.

(4) Adjust oxygen and acetylene flow to a neutral flame.

(5) Increase primary air flow to full open.

(6) Terminate combustion by cutting off fuel, then oxygen flow.

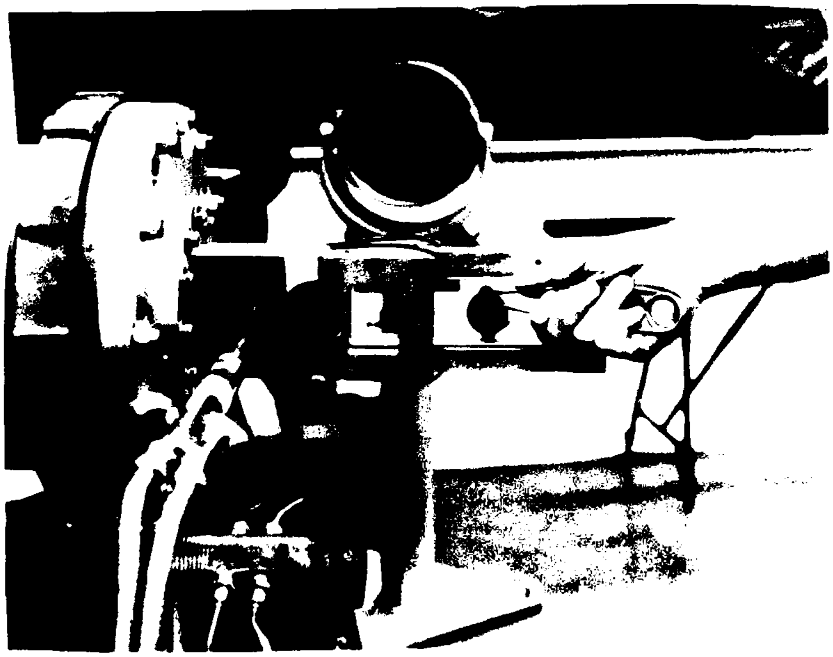

Figure 11. Igniting Test Section #4

Schlieren and normal color photographs were made of the flame and surrounding flow. Low ASA film was required for schlieren photography due to the light produced by the flame. The direct light from the flame was blocked off for some photographs by placing an opaque object over a portion of the window.

IV. Theoretical Model

The test cavity of all test sections represents the entrance to a supersonic combustor with no shocks in the inlet ducts. The sonic nozzles could represent the sonic exit of a subsonic combustor, or another parallel fuel injector where heat or mass addition would create a free boundary to turn and thereby diffuse the supersonic flow stream.

A base bleed model developed by Chow (10) and adapted to the geometry of test sections #1-#3 is seen in Figure 12. This model can be used with little or no secondary mass flow. Secondary flow is defined as flow from the sonic nozzle. In this model, the flow exiting the primary nozzle at Mach 3.02 would expand around the blunt end of the sonic nozzle block. Isentropic expansion theoretically accelerates the flow to Mach 3.34, due to the change in area, with zero secondary flow. A lip shock forms just beyond the corner due to the boundary layer separation at the corner. No lip shock forms if there is little expansion.

A recirculation, or base flow, region forms around the end of the sonic nozzle block, due to viscous effects. The velocity in the region is low, and pressure throughout the region is equal to the pressure on the end surface of

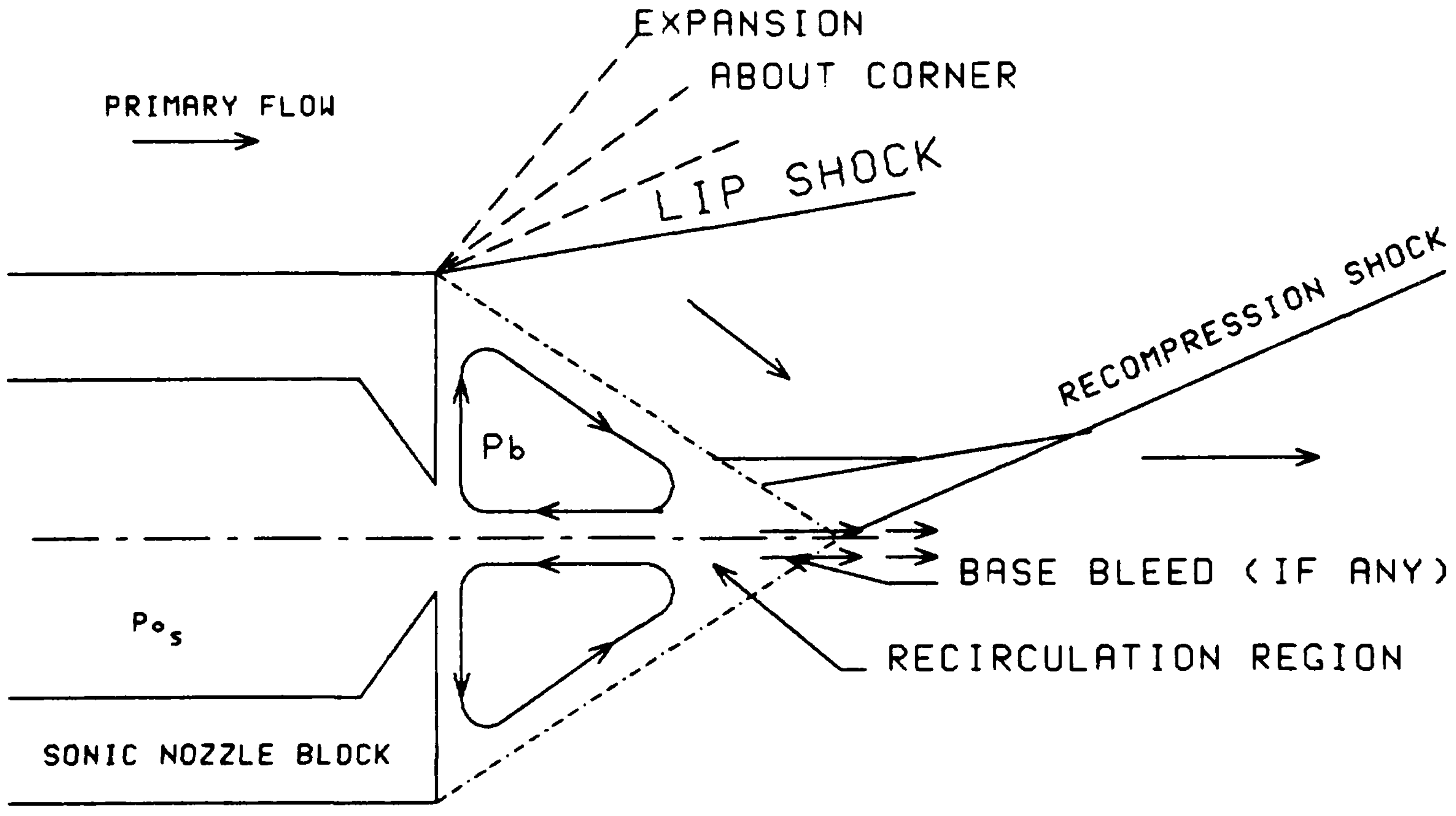
EXPANSION
ABOUT CORNER
PRIMARY FLOW
LIP SHOCK
RECOMPRESSION SHOCK
Pb
BASE BLEED (IF ANY)
RECIRCULATION REGION
P_{o_s}
SONIC NOZZLE BLOCK

Figure 12. Base Bleed Model

the nozzle block. This base pressure, P_b, is much lower than the static pressure at the nozzle exit plane.

An invicid flow model (9:37), the limiting case for a zero boundary layer thickness, predicts that base pressure between two Mach 3 flows approachs absolute zero, $P_b = .04$ psia for $Po_p = 100$ psia. However, viscous effects increase the base pressure. Korst theory (14:594) for supersonic flow past a back step predicts base pressure, $P_b = .46$ psia, for the same conditions. The theory of Crocco and Lees (11) includes the effects of turbulence on base pressure. A turbulent boundary layer, for moderate turbulence intensity, causes an increase in base pressure to approximately .3 times the nozzle exit static pressure, or .80 psia for the geometry and flow conditions of test sections #1-#3. Therefore, base pressure can indicate the nature of the boundary layer approaching the base region.

A slow bleed of air into the base region from the secondary nozzle can increase the base pressure. Any bleed air leaves the base region parallel to the centerline. As the total pressure feeding the base bleed exceeds the static pressure outside the recirculation region the bleed air is accelerated and approaches sonic velocity. A secondary, or bleed, total pressure, Po_s, of only 5 psia is required to cause sonic flow from a base region, surrounded by Mach 3 flow driven by a total pressure of 100 psia.

At the end of the recirculation region the flows from both sides meet at the recompression point. The recompression causes a shock in both flows that turns them back to their original direction. The increase in static pressure feeds back into the base region from the recompression point and increases the base pressure.

At secondary total pressures above 5 psia, the flow expands leaving the nozzle and accelerates to supersonic velocities. This expanding flow model, adapted from Chow's analysis (10), is seen in Figure 13. The base region is now reduced to only a small triangle at each step between the primary air nozzle and the sonic nozzle slot. The expansion of both streams turns the flow away from the nozzle centerline. This adjusts the static pressure of both streams to the base pressure, P_a. The base pressure is assumed to be constant and equal to the static pressure of both streams at the end of their expansion. The recompression at the end of the recirculation region, generates an interaction shock in both streams as they are turned back toward the centerline and parallel to each other. The interaction shock is defined here as a recompression shock that does not turn the flow back to the original flow direction. The angle of the flows after the recompression is the effective turning angle created by the expanding sonic jet interacting with the supersonic flow.

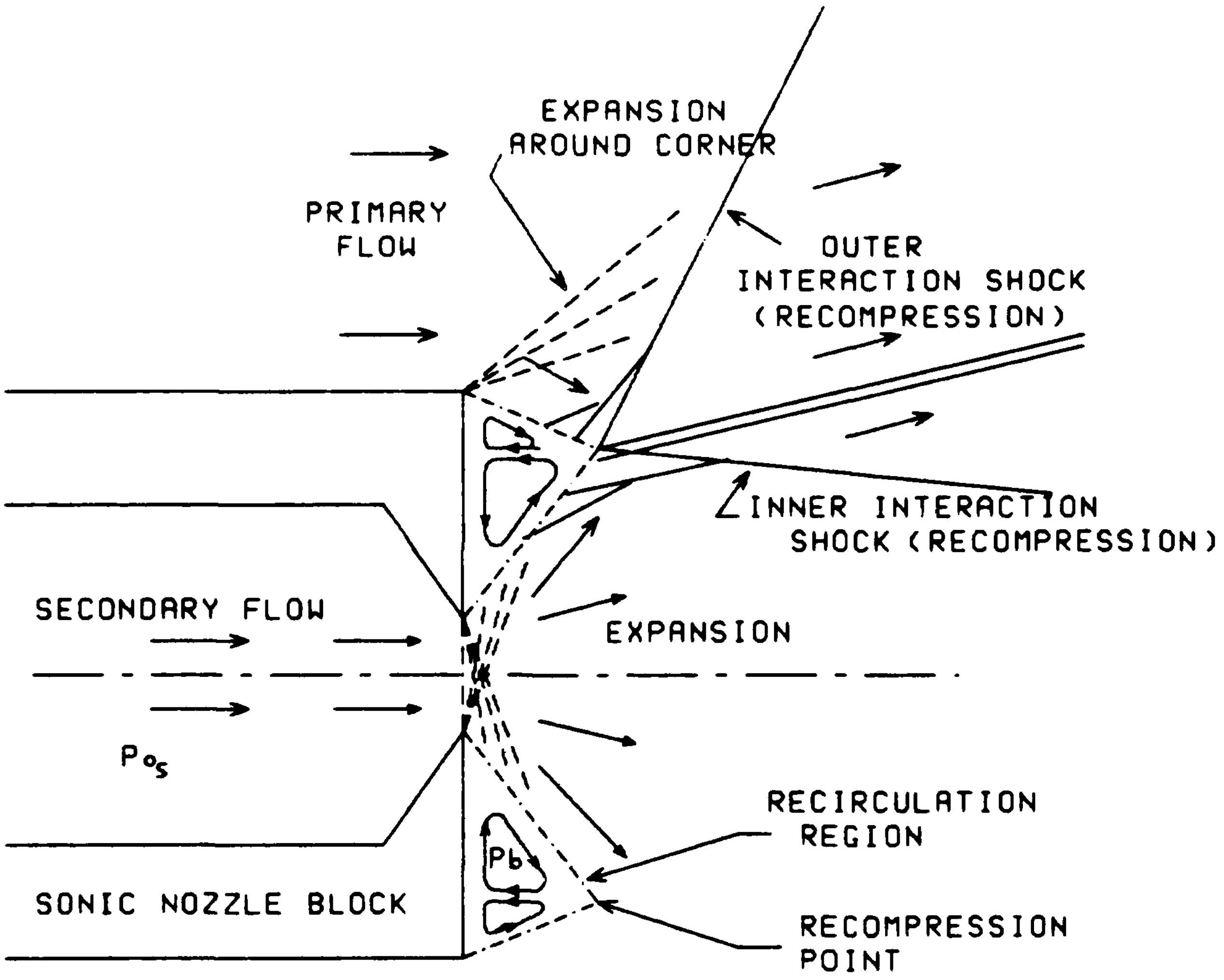
EXPANSION
AROUND CORNER
PRIMARY
FLOW
OUTER
INTERACTION SHOCK
(RECOMPRESSION)
INNER INTERACTION
SHOCK (RECOMPRESSION)
SECONDARY FLOW
EXPANSION
P_{o_s}
RECIRCULATION
REGION
P_b
SONIC NOZZLE BLOCK
RECOMPRESSION
POINT

Figure 13. Expanding Flow Model

A one-dimensional analysis was used by this author to predict the base pressure and the area of each nozzle stream in the test cavity. Each stream is allowed to expand from its nozzle exit until both flows fill the available area of the flow at equal static pressures. This may be calculated for a specified ratio of secondary- to primary-reservoir pressure by the following numerical method:

1) Guess the Mach Number of the sonic stream after it expands.
2) Compute the area ratio for this Mach number.
3) Subtract the area of this stream from the total area of the test cavity to determine the required area ratio of primary stream.
4) Compute the Mach number that corresponds to this area ratio.
5) Compute the ratio of static-to-total pressure for this primary stream.
6) Divide by specified ratio of reservoir pressures to find static-to-total pressure ratio in the secondary stream.
7) Compute the Mach number that corresponds to the ratio computed in 6.
8) Use this Mach number as next guess of Mach number, return to 2 and iterate to an acceptable tolerance.

A mass flux ratio, defined as the secondary mass flow per unit area divided by the primary mass flow per unit area, can be determined by assuming isentropic expansion of the two flows. For two flows of equal total temperatures, the mass flux ratio reduces to:

$$MFR = (A_p / A_p^*)(Po_s / Po_p) \; / \; (A_s / A_s^*)$$

A large mass flux ratio would be analogous to a large heat flux to a flow.

The results of this analysis, for the geometry of test sections #2 and # 3, are shown in Table 1 and Figures 14 and 15. This analysis predicts that a critical point for this test section occurs at a secondary- to primary-reservoir pressure ratio of about .55. At this ratio the primary stream no longer expands after leaving the nozzle exit. Higher secondary pressure ratios begin to compress the primary stream, decreasing primary Mach number, and base pressures continue to rise. This could be expected to continue until the base pressure becomes so large that it causes separation of the flow inside the primary nozzle.

The highest reservoir pressure ratio achieved by this investigation was less then .8. A ratio of .8 would accelerate the secondary flow to Mach 2.8 by one dimensional analyses. The recirculation region on both sides of the expanding flow provides an effective divergent section to the sonic nozzle. The Prandtl-Meyer

Table 1

One Dimensional Analysis of Test Sections #2 and #3 as Designed

GAMMA 1.4

	SECONDARY			PRIMARY		
PoS/ PoP	MACH	A/A*	P/Po	MACH	A/A*	P/Po
0.05	1.254	1.048	.38392	3.236	5.297	.01920
0.10	1.707	1.344	.20057	3.206	5.149	.02006
0.15	1.945	1.612	.13930	3.178	5.015	.02090
0.20	2.106	1.846	.10838	3.153	4.898	.02168
0.25	2.227	2.054	.08965	3.130	4.794	.02241
0.30	2.324	2.241	.07704	3.110	4.700	.02311
0.35	2.404	2.412	.06796	3.090	4.615	.02379
0.40	2.472	2.570	.06109	3.072	4.536	.02444
0.45	2.532	2.717	.05571	3.055	4.463	.02507
0.50	2.584	2.853	.05136	3.039	4.395	.02568
0.55	2.631	2.981	.04778	3.024	4.330	.02628
0.60	2.673	3.102	.04478	3.009	4.270	.02687
0.65	2.711	3.217	.04223	2.995	4.213	.02745
0.70	2.746	3.326	.04002	2.981	4.158	.02802
0.75	2.778	3.428	.03809	2.968	4.107	.02857
0.80	2.808	3.527	.03640	2.955	4.057	.02912
0.85	2.836	3.621	.03490	2.943	4.010	.02967
0.90	2.862	3.711	.03355	2.931	3.966	.03020
0.95	2.886	3.797	.03234	2.920	3.922	.03073
1.00	2.908	3.881	.03125	2.908	3.881	.03125
1.05	2.930	3.960	.03026	2.898	3.841	.03177
1.10	2.950	4.037	.02935	2.887	3.802	.03228
1.15	2.969	4.112	.02852	2.877	3.765	.03279
1.20	2.987	4.183	.02774	2.867	3.729	.03329
1.25	3.005	4.253	.02704	2.857	3.694	.03380
1.30	3.021	4.321	.02638	2.847	3.661	.03430
1.35	3.037	4.385	.02576	2.838	3.629	.03478
1.40	3.052	4.449	.02520	2.829	3.597	.03528
1.45	3.066	4.510	.02466	2.820	3.566	.03576
1.50	3.080	4.569	.02416	2.811	3.537	.03624
1.55	3.093	4.627	.02369	2.802	3.507	.03673
1.60	3.106	4.682	.02325	2.794	3.480	.03719
1.65	3.118	4.737	.02283	2.786	3.452	.03767
1.70	3.130	4.791	.02244	2.777	3.425	.03815
1.75	3.141	4.843	.02207	2.769	3.399	.03862
1.80	3.152	4.894	.02171	2.761	3.374	.03908
1.85	3.162	4.943	.02138	2.754	3.350	.03955
1.90	3.173	4.990	.02105	2.746	3.326	.04000
1.95	3.183	5.038	.02075	2.739	3.302	.04047
2.00	3.192	5.083	.02046	2.732	3.280	.04092

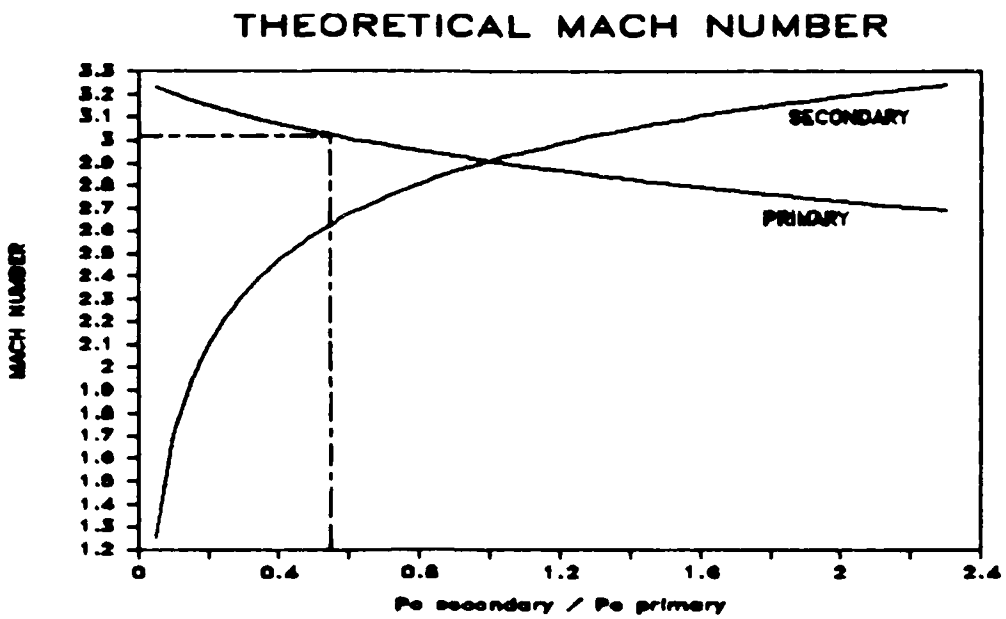

Figure 14. Theoretical Mach Number for Secondary and Primary Streams vs. Reservoir Pressure Ratio for Geometry of Test Sections #2 and #3

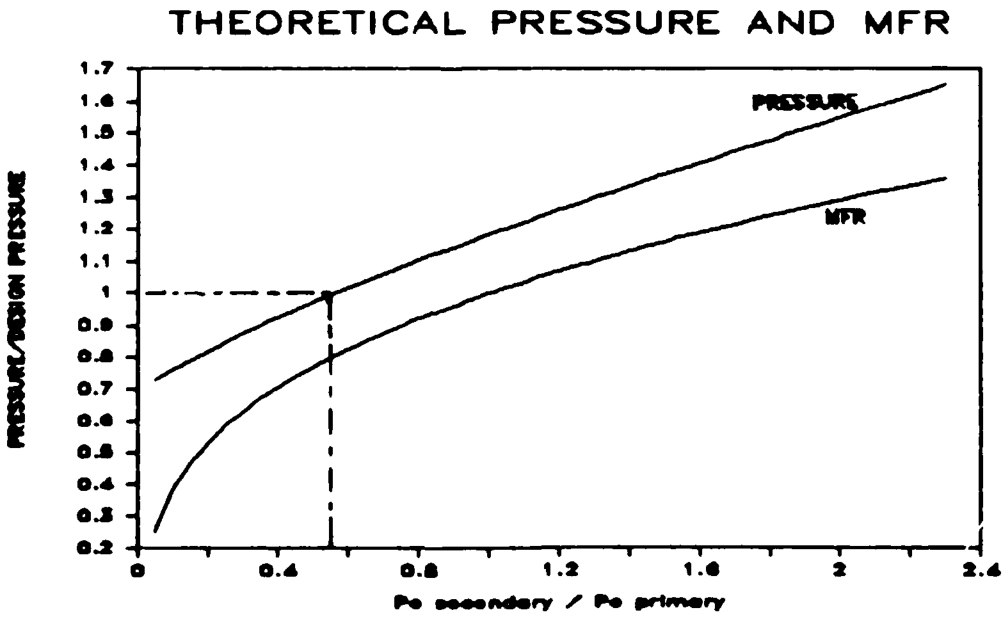

Figure 15. Theoretical Primary Flow Normalized Pressure and Mass Flux Ratio for Test Section #2 and #3

turning angles required to accelerate the sonic flow to Mach 2.8 would be over 45 degrees. Therefore, an accurate two-dimensional solution for this rapidly expanding secondary flow stream would require a fine mesh and be very difficult, without relying on a computer solution. The one dimensional analysis is not valid near the sonic nozzle due to the rapid expansion, but should be fairly accurate near the recompression point. The one dimensional analysis does not predict the curved flow boundaries seen in the optical investigation. However, this one dimensional analysis of the expanding flow model was helpful in understanding the experimental results.

V. Results and Discussion

The experimental data collected consisted of static and pitot pressure measurements and schlieren photography on all test sections. Normal optical photos were also used to record the flame investigation of test section #4.

Pressure Measurement Data Reduction

A pitot tube placed in supersonic flow causes a curved bow shock to form in front of the pitot tube. The ratio of the total pressure just behind the shock to the static pressure just upstream and undisturbed by the shock, Po_y/P_x, is used to find the Mach number just ahead of the bow shock.

The measured pitot pressure is Po_y, assuming the flow is parallel to the tube (22:153-154). The static pressure measured on the sidewall of the cavity is P_x, assuming static pressure is constant across the thickness of the test cavity. After forming the ratio Po_y/P_x, the Mach number was computer calculated by iteration of the Rayleigh pitot-tube formula to a tolerance of ±.001. The actual total pressure, Po_x, was calculated by isentropic relationships from the sidewall static pressure and the Mach number.

Boundary layer effects invalidated calculated Mach number and total pressure where measurements were made in the vicinity of a strong shock wave. The pressure is "diffused" upstream and downstream through the boundary layer near the sidewall (21:358-372, 23:1138-1142). Therefore, the assumption that static pressure is constant across the depth of the test cavity is not valid near strong shocks. Experimental evidence (21:361-363) suggests the width of diffusion is 100 times the thickness of the boundary layer for laminar flows, and 10 times for turbulent flows. Diffusion of the pressure gradient due to a strong shock may separate the boundary layer in front of the shock. For example, a pressure ratio of 1.8, which corresponds to an oblique shock that turns a Mach 3 flow nine degrees, may separate a turbulent boundary layer. A separated boundary layer on the sidewall could cause a separation "bubble" on the sidewall which would generate shocks and expansion waves across the thickness of the nozzle (23:1140). The flow then becomes increasingly less two-dimensional.

The pitot probe tip was moved across the depth of the test cavity and a 2-4 psi variation in pitot pressure was noted. This suggests a variation in the velocity across the depth of the channel caused by boundary layer effects.

The boundary layer seen on the nozzle wall measured .5 millimeters thick. A turbulent boundary layer .5mm thick on the sidewall would diffuse .2 inches upstream of the shock. Figure 16 depicts sidewall static pressures measured in test section #2 every .107 inches along the centerline of the upper primary nozzle. The pressure begins to rise .107 to .214 inches ahead of the shock location, as determined by schlieren photographs for the same flow conditions. This caused the static pressure on the sidewall to be higher than the pressure in the cavity ahead of the shock, and lower than that in the cavity behind the shock. Any Mach numbers and total pressures calculated by the Rayleigh pitot tube formula with Po_y and P_x measurements in a region affected by a shock wave were obviously in error. This was clearly demonstrated in this study by the fact that some calculated total pressures, Po_x, were greater then reservoir pressure.

Static pressure measurements were very repeatable. Differences in sidewall static pressure measurements between runs for the same flow conditions were normally less than .1 psi. This is of the same order of magnitude as the noise in the analog-to-digital converter. Pitot pressure measurements were less repeatable. Differences of 5%-8% between two pitot pressure measurements, at the same location, near a shock were common. However, measurements further from a shock differed by less than 2%. Differences may have been due to inaccurate manual positioning of the probe.

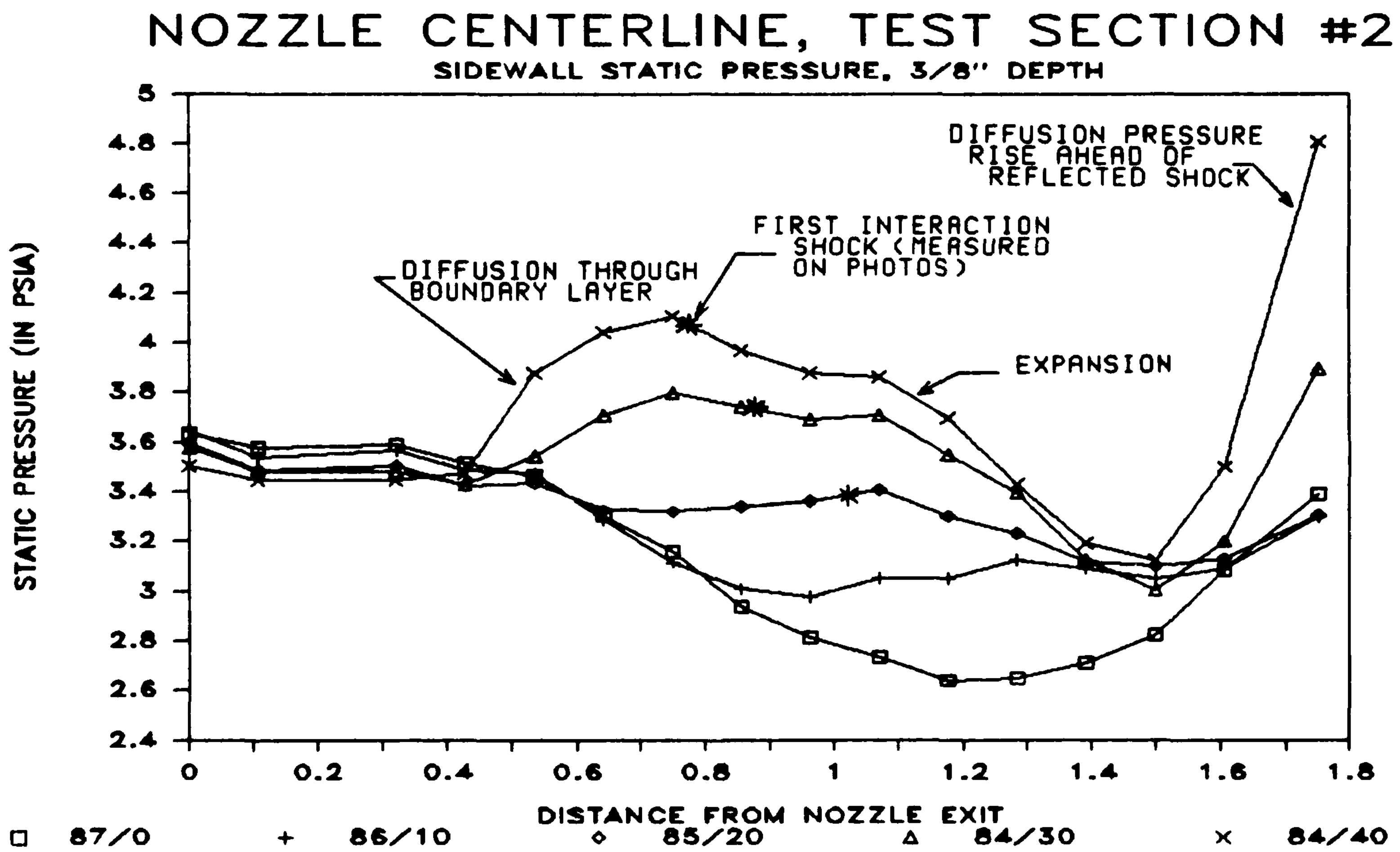

Figure 16. Upper Primary Nozzle Centerline Pressures, Showing Diffusion Through Boundary Layer

Results From Optical Study

Shock angles were measured from the schlieren photographs. From these measurements, turning angle of the flows can be determined by oblique shock relationships if the upstream Mach number is known. The flow direction between the interaction shocks behind the sonic nozzles can be seen in the photos, Figures 17-20, as indicated by turbulence along the shear layer between the flows. Measurements of the flow direction agreed with the turning angle expected from measured exit Mach and shock interaction angle. At low reservoir pressure ratios, Po_s/Po_p, the secondary flow stream behind the sonic nozzle block did not expand to the height of the nozzle block itself. This is as expected from predictions by the one dimensional flow model. Figure 13 illustrates this flow condition. As the reservoir pressure ratio, and hence, secondary flow expansion increased, the shear layer turbulence between flows became much less apparent.

As the reservoir pressure for the sonic nozzle, Po_s, increased, the interaction shock angle increased, implying that the shocks grew stronger. This can be seen by comparing the photographs in each figure, Figure 17-20, with increasing sonic reservoir pressure. The one dimensional analysis of the expanding flow model predicts the larger shock angle because the area of the flow from the sonic nozzle increases with increasing reservoir

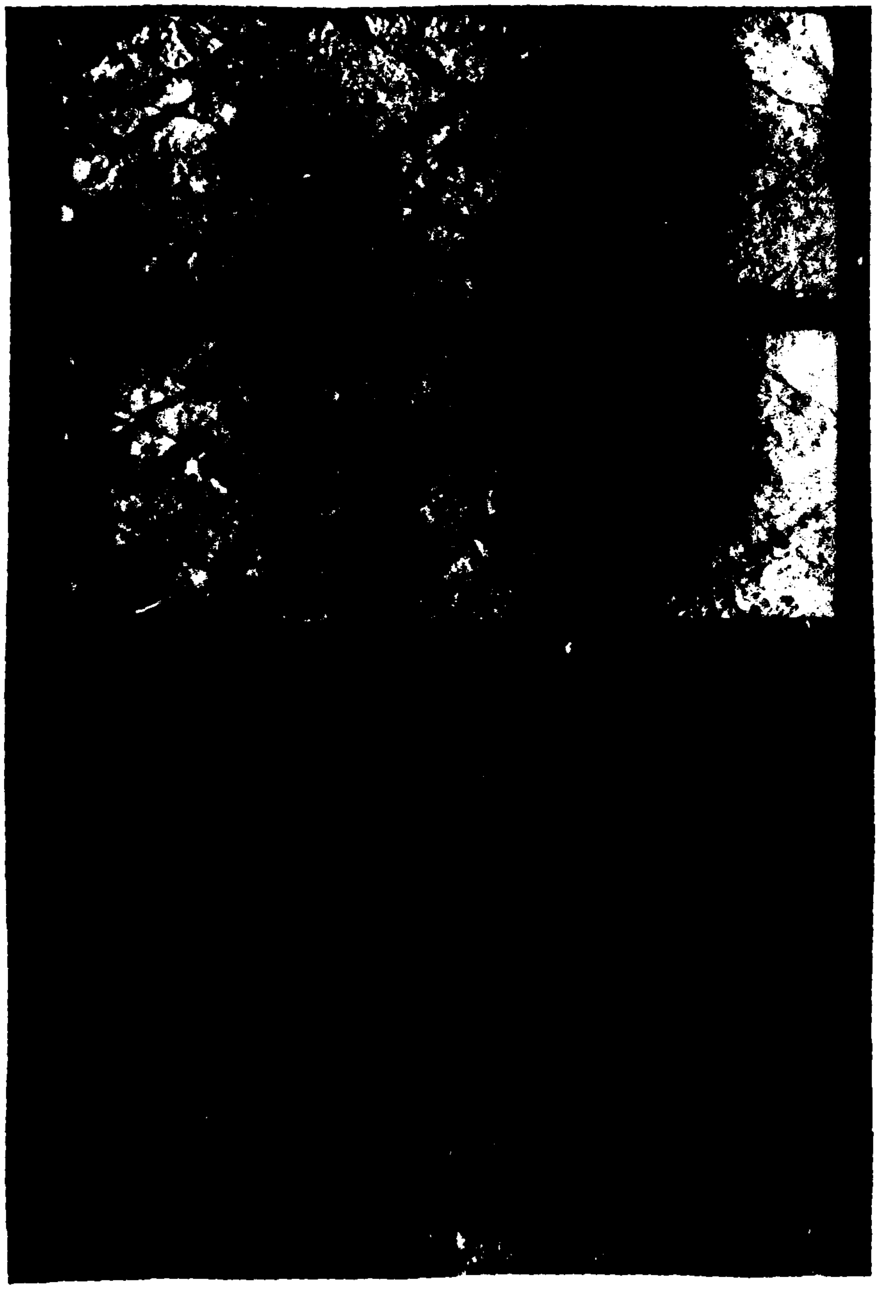

Figure 17. Composite Schlieren Photographs of Flow in Test Section #1 with Primary/Secondary Reservoir Pressure of:
(a) 75 psig / 50 psig (b) 84 psig / 22 psig
(c) 84 psig / 10 psig (d) 84 psig / 0 psig

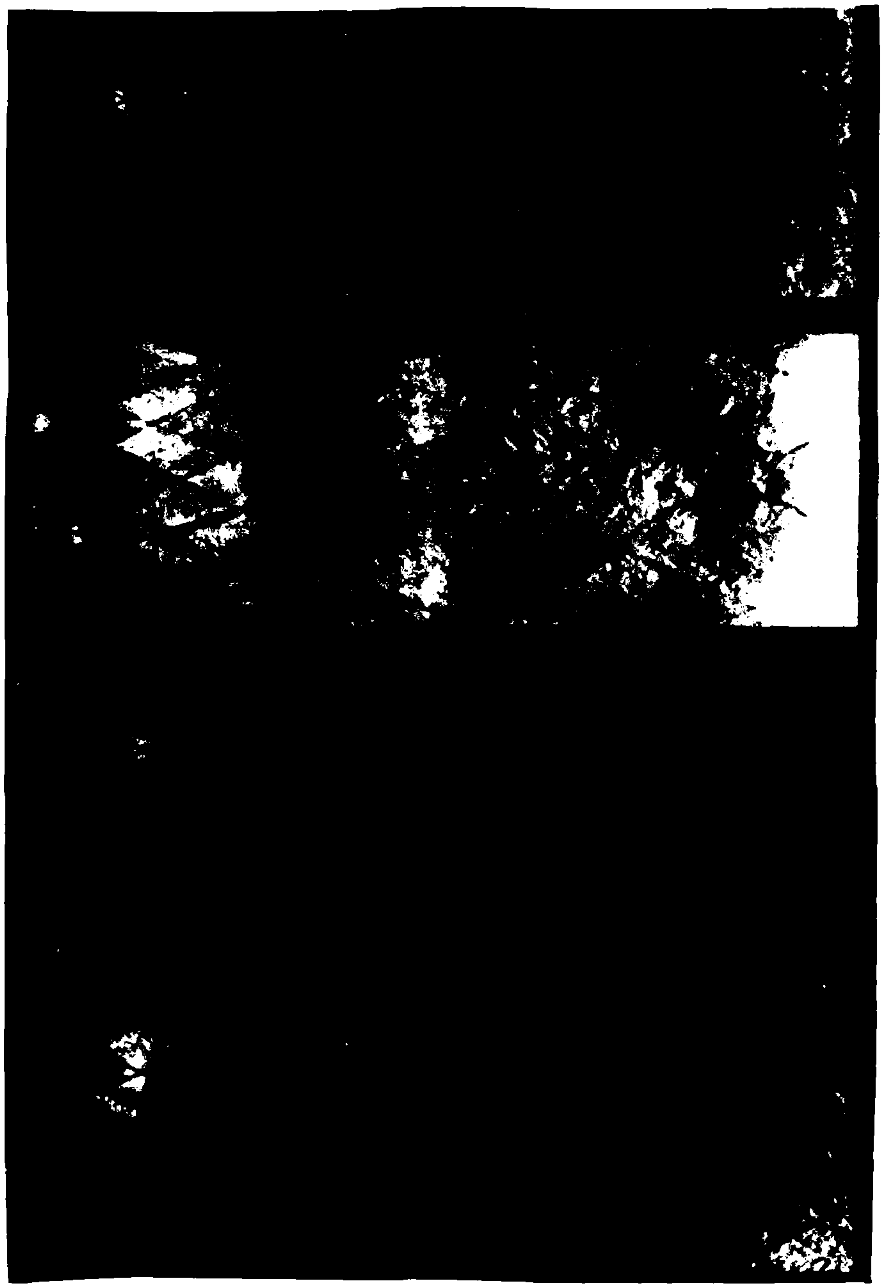

Figure 18. Composite Schlieren Photographs of Flow in Test Section #2 with Knife Edge Perpendicular to Flow Direction with Primary/Secondary Reservoir Pressure of:
(a) 85 psig / 10 psig (b) 84 psig / 20 psig
(c) 83 psig / 30 psig (d) 82 psig / 40 psig

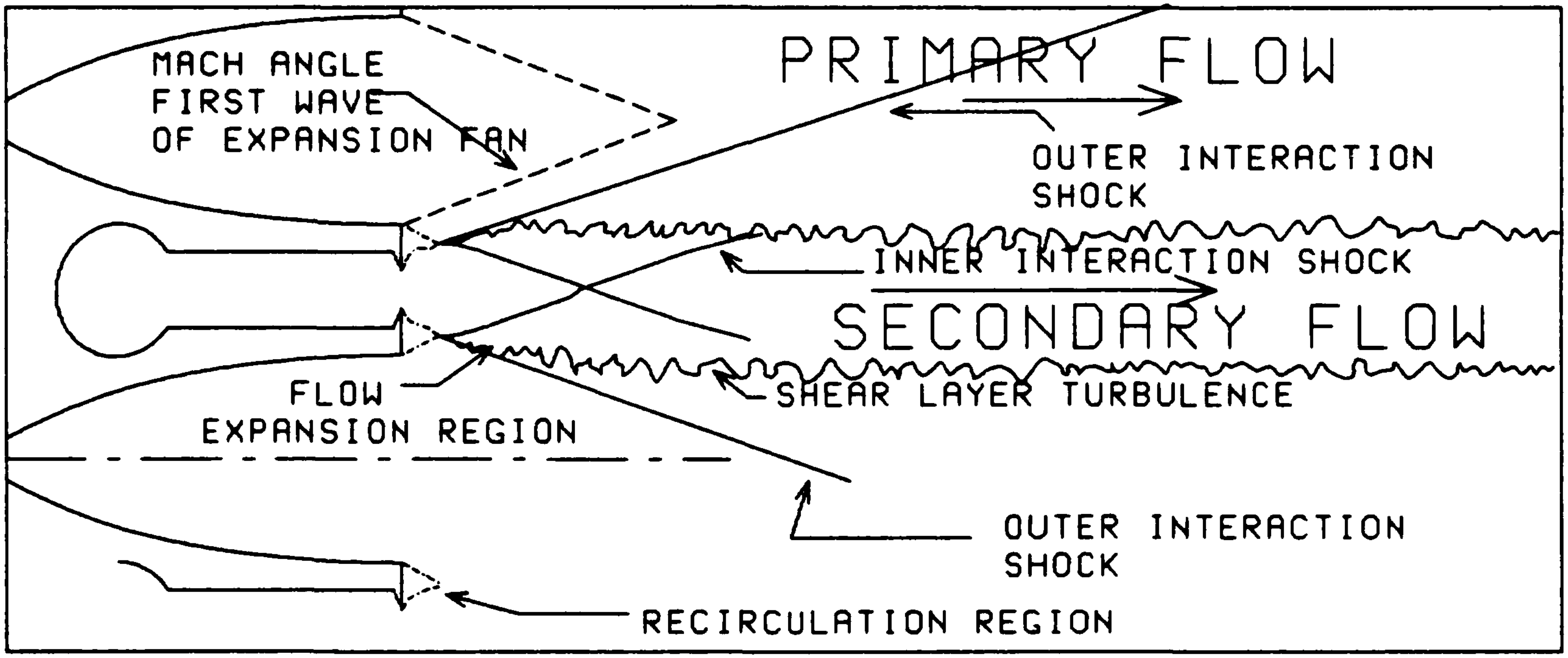
MACH ANGLE
FIRST WAVE
OF EXPANSION FAN
PRIMARY FLOW
OUTER INTERACTION
SHOCK
INNER INTERACTION SHOCK
SECONDARY FLOW
FLOW
EXPANSION REGION
SHEAR LAYER TURBULENCE
OUTER INTERACTION
SHOCK
RECIRCULATION REGION

Figure 18e. Nomenclature for Photograph Description

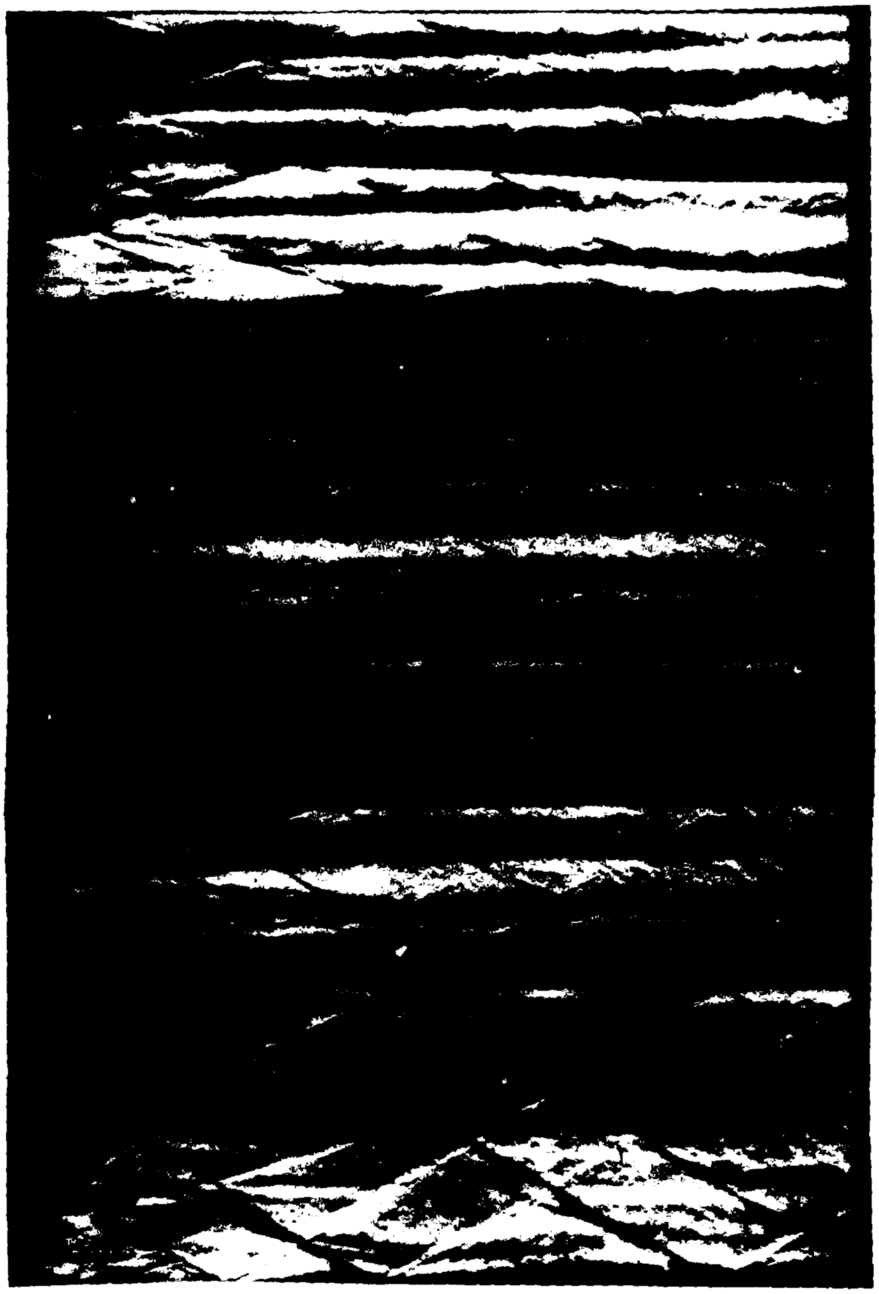

Figure 19. Composite Schlieren Photographs of Flow in Test Section #2 with Knife Edge Parallel to Flow with Primary/Secondary Reservoir Pressure of: (a) 87 psig / 0 psig (b) 85 psig / 10 psig (c) 84 psig / 22 psig (d) 79 psig / 58 psig

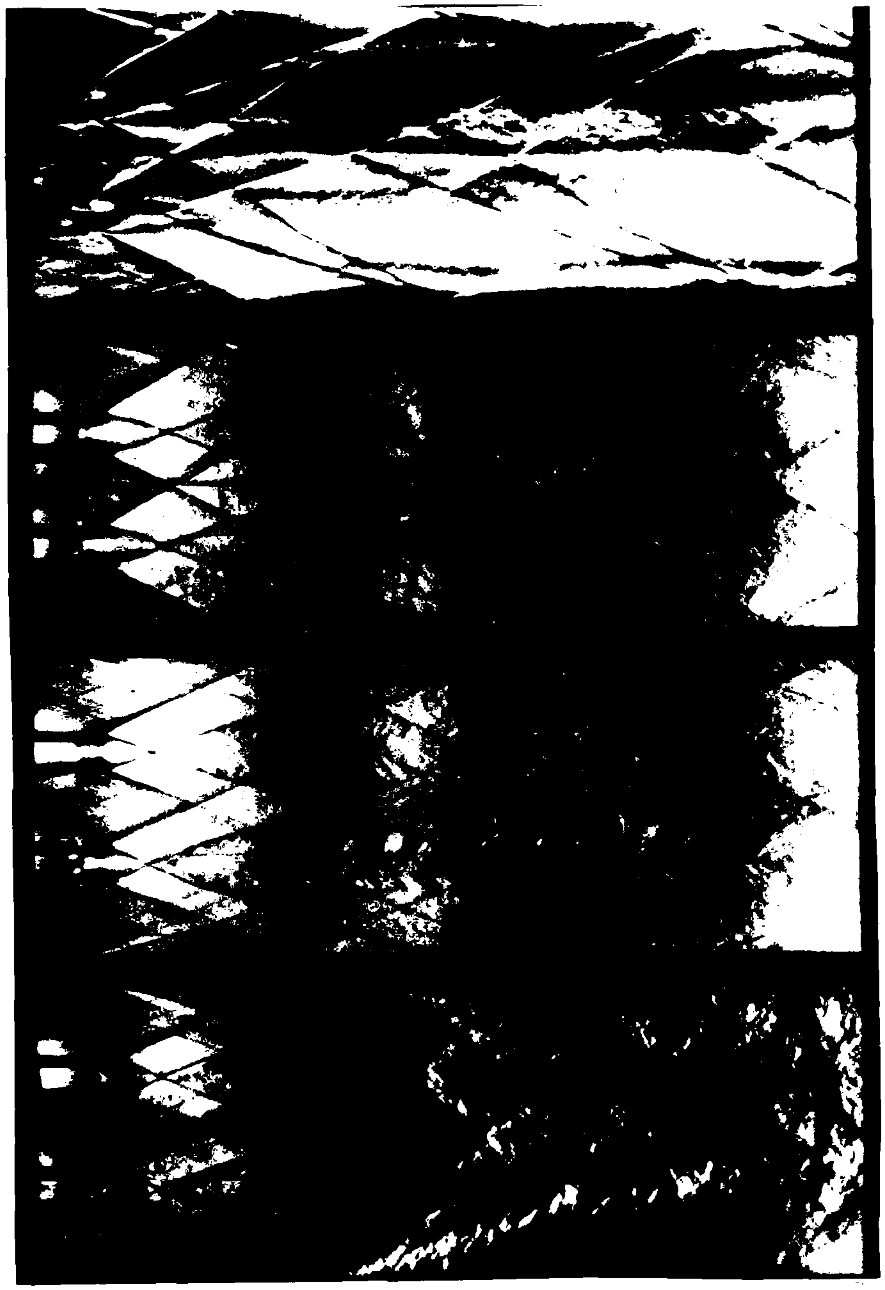

Figure 20. Composite Schlieren Photographs of Flow in Test Section #3, Knife Edge Parallel in (a) only, with Primary/Secondary Reservoir Pressure of:
(a) 67 psig / 32 psig (b) 67 psig / 32 psig
(c) 69 psig / 15 psig (d) 70 psig / 10 psig

pressure ratio, therefore, the primary flow must be turned more to decrease its area.

Effects of Nozzle Geometry-Test Section #1

Mislocation of the nozzle blocks in test section #1 created a .110 inch throat, instead of .133 inches. The resulting off-design versus design configuration is seen in figure 21. Two nozzle walls placed at the designed distance from each other will turn the expanding flow back parallel to the axis and exactly cancel the expansion wave that originated at the sharp corner throat. In the off-design configuration the walls are too close together. The slope of the wall does not turn the expanding flow completely back to parallel and the expansion wave is reflected off the wall. The result is non-uniform flow at the nozzle exit.

Pitot pressures measured across the primary nozzle exit plane varied from 30 psia to 13 psia. This confirmed the non-uniform flow. The expansion waves from the nozzles also made accurate measurement of pitot pressures near the nozzle exit difficult.

The preliminary investigation on test section #1 revealed that stablity of the flow within the test cavity was very sensitive to the amount of secondary mass flow. The schlieren pictures, shown in Figure 17, revealed that a secondary- to primary-reservoir pressure ratio of 18 psig/85 psig, or $Po_s/Po_p=.325$ was required for a stable

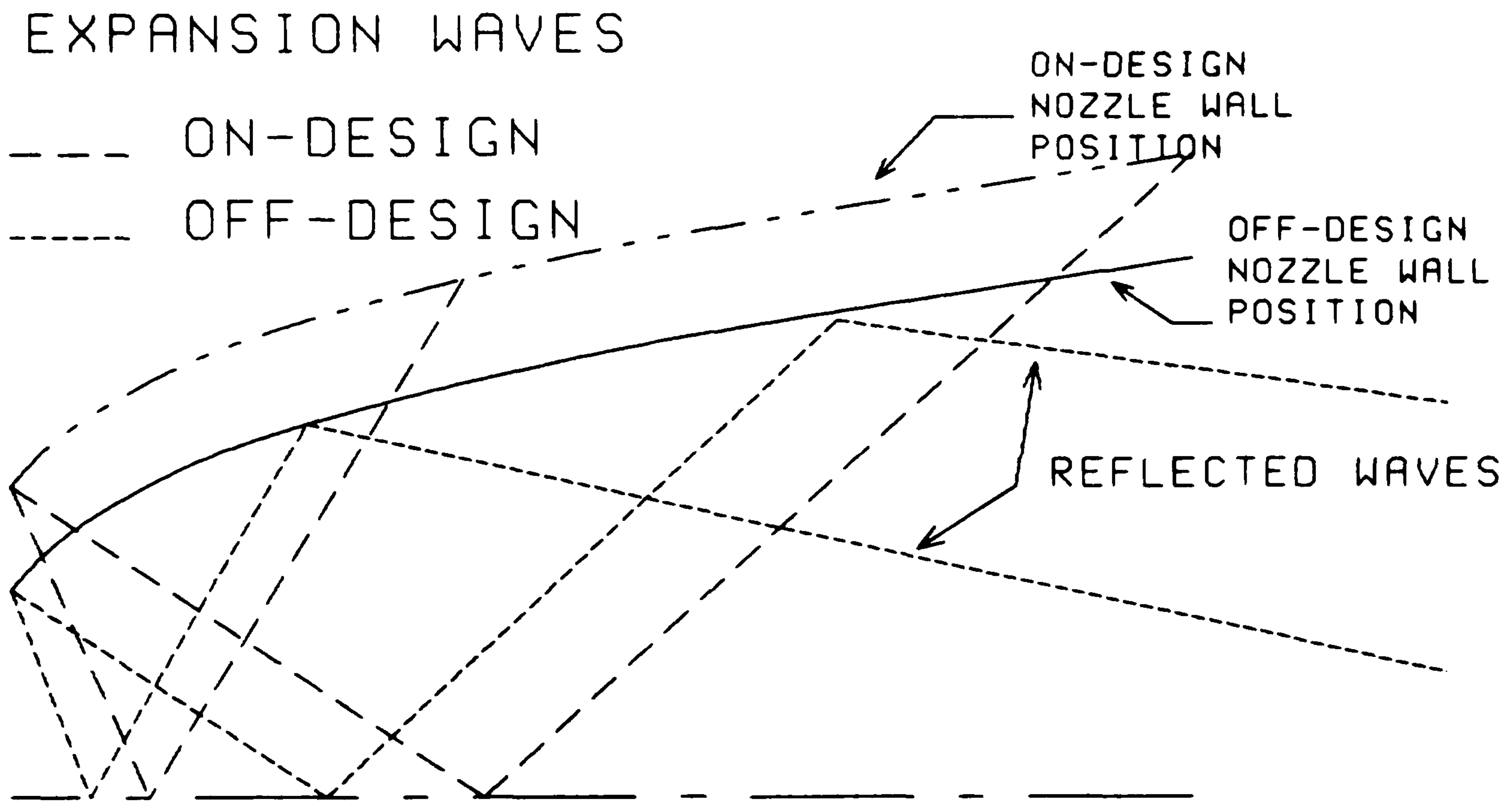
EXPANSION WAVES
ON-DESIGN
OFF-DESIGN
ON-DESIGN NOZZLE WALL POSITION
OFF-DESIGN NOZZLE WALL POSITION
REFLECTED WAVES

Figure 21. Off-Design Nozzle Configuration

flowfield. This was also the approximate pressure ratio where the interaction shock angle was equal to the Mach angle, seen as the first wave of the expansion fan in the schlieren photographs. This is seen in Figure 17b. Above this pressure ratio, the flowfield was always stable, as seen in Figure 17a. Below this pressure ratio, the stream from the center primary nozzle would occasionally oscillate at high frequency, alternately attaching and detaching from the upper, then lower primary stream. It is seen off-center in Figure 17d. Figure 17c shows a steady flow condition at an intermediate secondary- to primary reservoir pressure ratio, 10 psig/84 psig. This condition would remain stable for a few seconds and then the center stream would begin oscillating.

Turbulence is also clearly seen in the flowfield, especially near the interaction shocks. Turbulent kinetic energy is an important factor in mixing rates (20). Therefore, increased turbulence increases mixing between the two flows because, at least initially turbulent kinetic energy is increased. However, an off-design nozzle is an inefficient method of increasing mixing due to a large total pressure loss.

The total pressure loss can be seen by comparing average pressure measurements for identical reservoir pressures between test sections #1 and #2, from Tables 4 and 5 in the appendix. The total pressure loss, averaged for the three nozzles and averaged for all runs with test section #1, was 36% at the nozzle exit plane, and 60% 2.75 inches behind the nozzle exit. This compares with 15% and 39% respectively for test section #2, which has correct nozzle geometry.

The pressure measurements reveal a variation of pitot and static pressures along the axis of the center nozzle as reservoir pressure ratio increases. The pressures, at the highest reservoir pressure ratio tested, are extracted from Table 7 in the appendix. They vary with distance from the nozzle exit as follows:

Distance from Nozzle Exit (in)	Pressures (Psia) Static	Pitot
0	3.91	35.19
.75	8.13	41.25
1.75	2.06	18.87
2.75	4.09	25.86
3.75	5.11	23.65
4.75	6.03	25.24

This indicates each shock is followed by an expansion and then another shock.

A view of the nozzle area alone, Figure 22, clearly shows the triangular base regions, predicted in Figure 13, at the end of the nozzle block, above and below each sonic nozzle. The curved boundary of the base region facing the sonic nozzle provides an effective divergent portion to the sonic nozzle. An inner, and an outer, interaction shock are produced at the recompression end of the base region. The inner interaction shock is almost parallel to the centerline at the recompression point. It curves

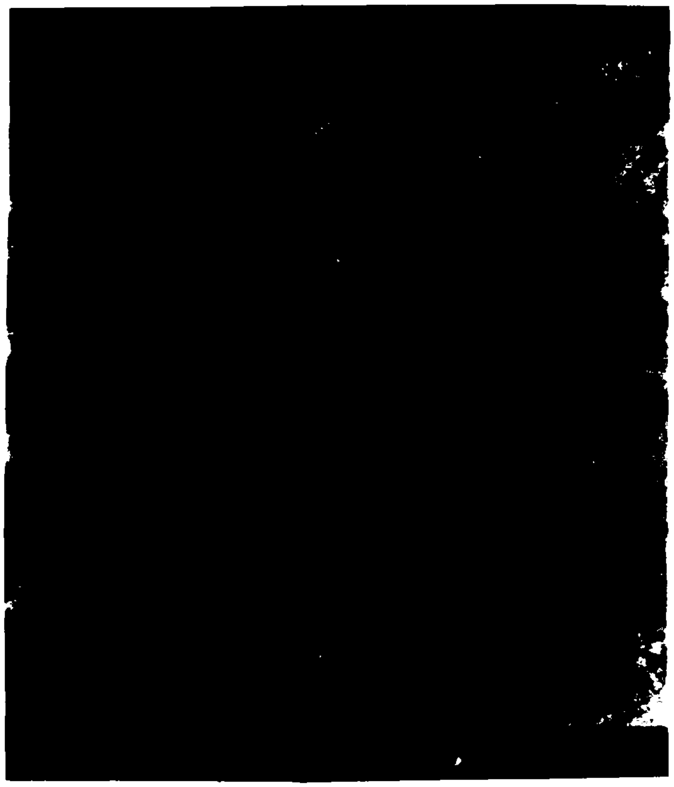

Figure 22. Schlieren Photograph of the Nozzle Area of Test Section #1 Po_p/Po_s = 86/55 psig

toward the centerline as it crosses expansion waves from the sonic nozzle. It crosses the shock from the base region on the other side of the nozzle near the nozzle centerline. From Figures 17-20 it can be seen that the area between these two inner interaction shocks increases as secondary pressure increases.

The outer interaction shocks on the outside of the sonic nozzle are nearly straight lines. These straight interaction shocks are distorted as they cross the expansion waves from the off-design primary nozzle. It is also apparent that the flow between the straight and curved interaction shocks is turned outward from the centerline at a small angle, thus diffusing the supersonic primary flow.

Test Section #2

The 3/8" test section with proper nozzle geometry produced a much more organized flow pattern. The flowfield was always stable with a repeatable symmetric flow. Even with no sonic flow, the oscillations of the center nozzle jet observed in test section #1 were not seen in the schlieren photographs of test section #2, Figures 18 and 19.

The photographs in Figure 18, with knife edge perpendicular to flow, and Figure 19, with knife edge parallel to the flow, show the flowfield with this test section. Turbulence was greatly reduced from that in test section #1. Expansion fans from the expansion around the base are clearly seen as a "W" shape, with the center of the "W" on the sonic nozzle.

The outside interaction shocks are now sharp, straight lines. The flow between the curved inner interaction shock and the outer interaction shock is turned outward at a noticably greater angle as the sonic reservoir pressure increases. This was predicted by the expanding flow model, and illustrated in Figure 13. The expanding flow appears, as seen in all pictures of Figure 18, to be turned parallel before the stream is crossed by the curved shock from the other side of the sonic nozzle.

In Figure 18a, the interaction shock on the upper nozzle is at an angle less than the exit Mach angle. The schematic of Figure 18e, which displays the nomenclature used to describe the photographs, also illustrates this flow condition. The secondary flow is narrower than the sonic nozzle block itself. The shear layer between the primary and secondary flows creates turbulence that is easily seen. The reflected shocks crossing the sonic nozzle centerline farther downstream curve toward the centerline indicating a much lower velocity stream. In Figure 18b, the interaction shock angle is nearly the same as the Mach angle.

Figure 18c shows flow conditions near the critical reservoir pressure ratio determined by the one dimensional model. The flow from the sonic nozzle is approximately the same height as the sonic nozzle block at this flow condition because the expanding jet just fills the area behind the nozzle block. The shocks crossing the sonic nozzle centerline farther downstream are nearly straight as the velocity difference between the two flows becomes less. With higher secondary reservoir pressures, as in Figure 18d, the interaction shock created from the effective wedge angle of the expanding sonic jet becomes stronger as the flow behind the sonic nozzle spreads compressing the primary stream.

Figure 19 depicts increasing secondary flow in test section # 2 with the knife edge parallel to flow direction. The sonic nozzle reservoir pressure is increased from zero in Figure 19a to the maximum available in Figure 19d. The darker area behind the sonic nozzles indicates a lower velocity air stream. These are more noticeable at low sonic reservoir pressures. As that pressure increases, the flow field becomes increasingly two dimensional as indicated by the deflection of the dark streams by shocks.

Test Section #3

Pictures of flow through the 5/8" deep test section are in Figure 20. Figures 20a and 20b are both of the maximum available secondary to primary reservoir pressure ratio, Po_s/Po_p. The difference in the knife edge position allows different details to be seen. In Figure 20b the spreading of the sonic jet can be seen between the two interaction shocks and is more prominent than in Figures 20c and 20d. At the recompression point, the angle of the flow is about 12 degrees from centerline, the average of the two shock angles. However, it corresponds to a wedge turning angle of only 8 degrees. The flow then curves back to parallel. Figure 20c depicts flow at the lowest secondary reservoir pressure for which flow in the test section is fully started, and not influenced by the ambient exit pressure, which was atmospheric pressure. A further reduction in secondary mass flow, seen in Figure 20d, caused normal shocks to form in the test section upstream of the diffuser.

The static pressures along the nozzle centerlines, for flow conditions seen in Figures 20a and 20b, are compared in Figure 23. The center primary nozzle stream experiences a compression and expansion pattern, corresponding to the highly two-dimensional flow created by the intersections of the strong interaction shocks and expansion after the shocks. It is clear that expansion waves, as well as shocks are reflecting through the test cavity.

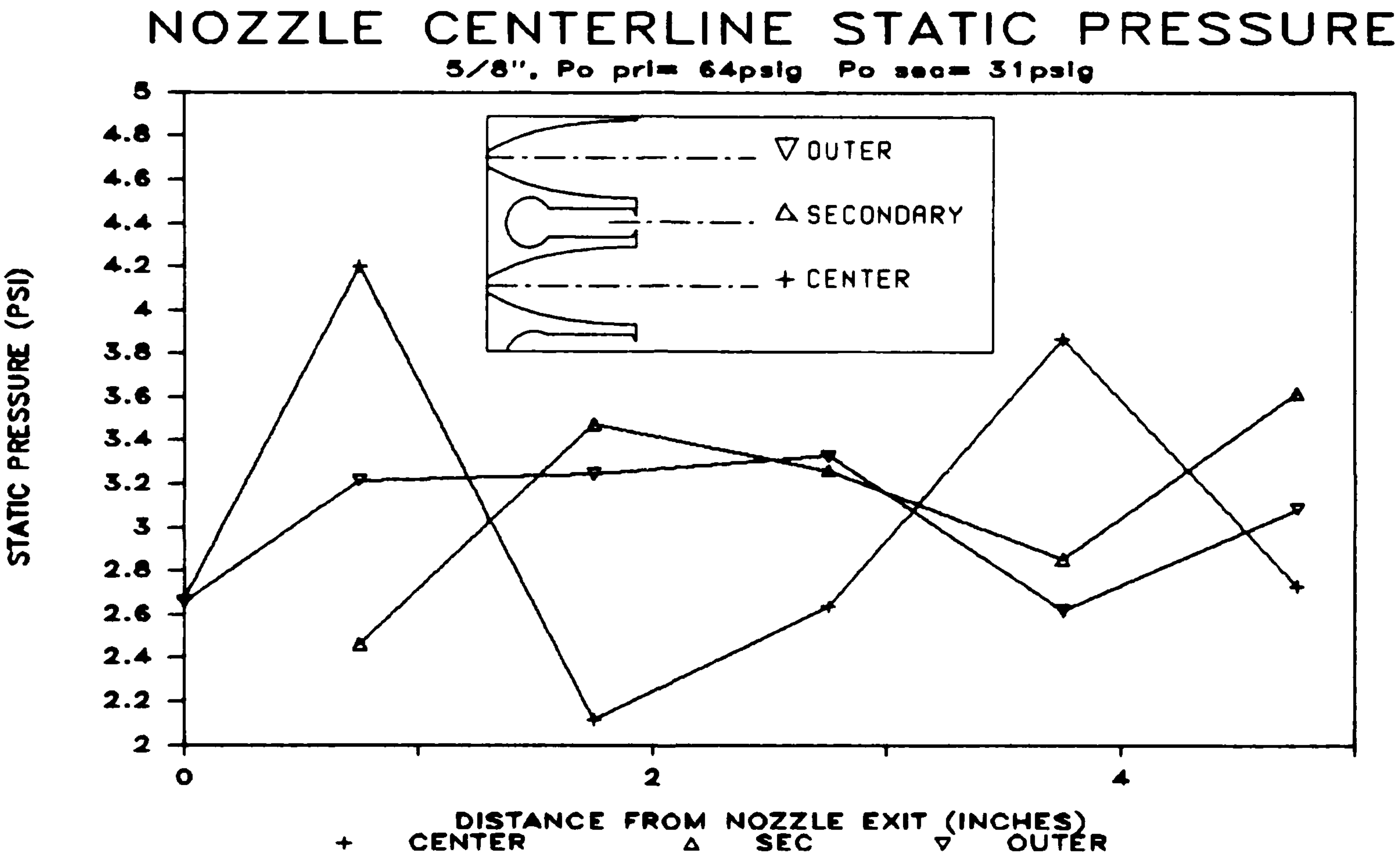

Figure 23. Test Section #3 Nozzle Centerline Static Pressure

One test run was made after a larger orifice was placed in the supply line. This allowed runs at the same secondary, Po_s, and primary reservoir pressures, Po_p, as available with test sections #1 and #2. However, at low secondary pressures, ambient exit pressure still produced normal shocks in the test section. This is evidence the boundary layers acted as a diffuser in test section #2, but had less effect on this deeper test section.

Exit Mach Number

The primary nozzles of the two test sections also had different exit Mach numbers, probably due to boundary layer effects. An attempt was made to determine exit Mach number of test section #2, using Figure 19a. The first notable wave of the expansion fan at the nozzle exit was at approximately 20 degrees from centerline, which corresponds to a Mach number of 2.92. With no flow from the sonic nozzle, the expansion fan ended with a lip shock originating from the corner at the end of the nozzle.

The pitot probe was placed in the nozzle exit plane on the centerline of the center nozzle with its tip about .100 inches from the wall, instead of at the center of the cavity. The angle of the bow shock measured 25.5 degrees, corresponding to a Mach number of 2.32. A difference of 2-4 psi pitot pressure was also noticed.

Static pressure measurements should be accurate in the nozzle exit plane, due to the absence of strong shocks. The average nozzle Mach number calculated from the pressure measurements was 2.65, for the nozzles of test section #2. A possible explanation for this is that the velocity profile is not uniform across the thickness of the test cavity due to viscous effects. The boundary layer would reduce the effective area ratio of the nozzle and cause a total pressure loss, and higher nozzle exit static pressure than that expected for isentropic, invicid expansion.

A boundary layer only .6mm thick on all exit surfaces, assuming no boundary layer at the throat would reduce the area ratio from 4.3 to 3.48, or a Mach number of 2.80, insteaad of 3.02. The boundary layer would actually be more elliptical in shape than rectangular at the nozzle exit cross section, due to an increased thickness in the corners. The decreased area ratio would cause a higher static pressure at the exit than would be expected without boundary layer. The nozzle exit static pressures measured in test sections #2 and #3 are compared with theoretical isentropic expansion of air in the primary reservoir to Mach 3 in Figure 24. The displacement effect of the boundary layer, along with entropy increases due to sharp throat expansion and friction, would account for this higher static pressures.

Base pressures were also measured in conjunction with measuring the pitot pressures. The pitot probe measured

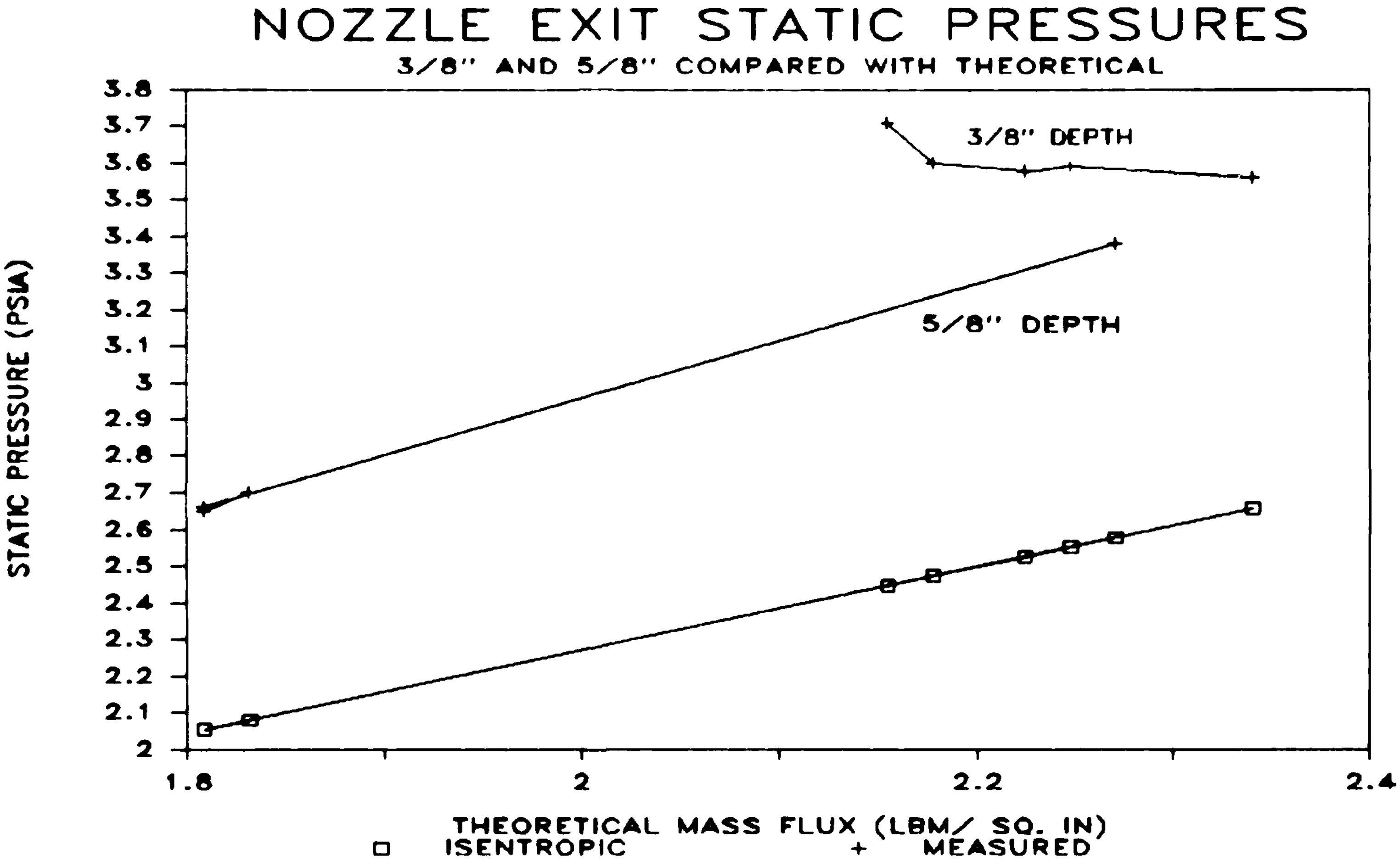

Figure 24. Nozzle Exit Static Pressures for Test Sections #2 and #3 Compared with Isentropic

the static pressure in the dead air region, only a few thousandths of an inch from the blunt end of the nozzle block. The measurements are compared with that predicted by one dimensional analysis in Figure 25. The base pressures were significantly lower than predicted. Nash's two dimensional analysis (16) explains underprediction in terms of boundary layer thickness approaching the base. Flow velocities in the recirculation region may not have been small, and a pressure gradient may exist between the solid boundary and the recompression point. These effects were not accounted for in this author's theoretical analysis.

The total pressure loss through the primary nozzles, averaged for all runs, was 15% for test section #2, and only 7% for the deeper test section #3. The calculated exit Mach numbers are assumed to be an accurate average of the Mach number across the stream. The calculated Mach numbers were 2.65 and 2.8 for test sections #2 and #3 respectively.

Shock Interaction Measurements, Test Sections #2 and #3

The angle of the outer interaction shocks measured from the nozzle centerline, which is the direction of primary flow before the shock, was measured to allow calculation of an equivalent wedge angle for the turning effect of the expanding jet. In Figure 26 the angle measurements from both test sections are compared versus

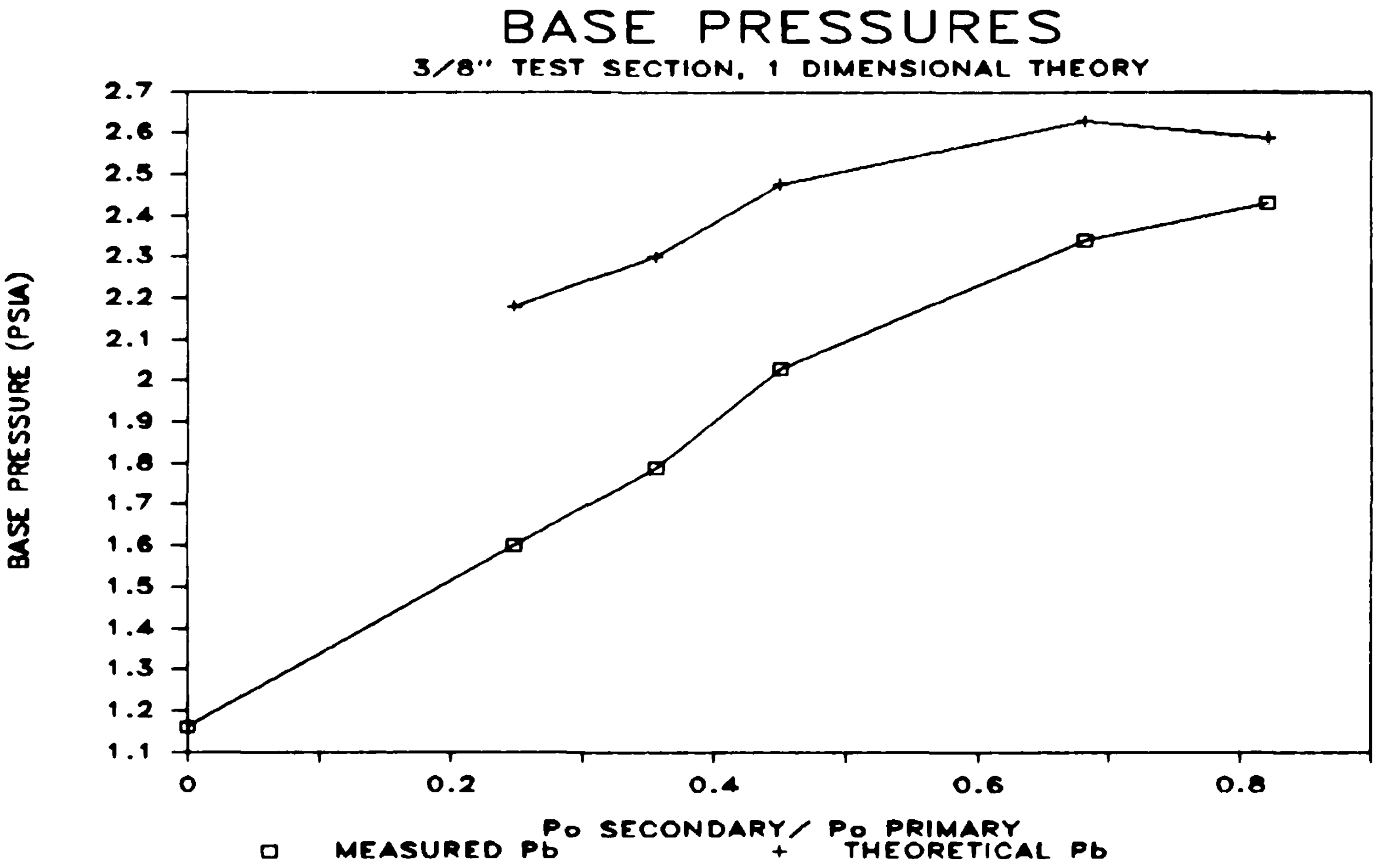

Figure 25. Measured Base Pressures, Compared with One Dimensional Theory

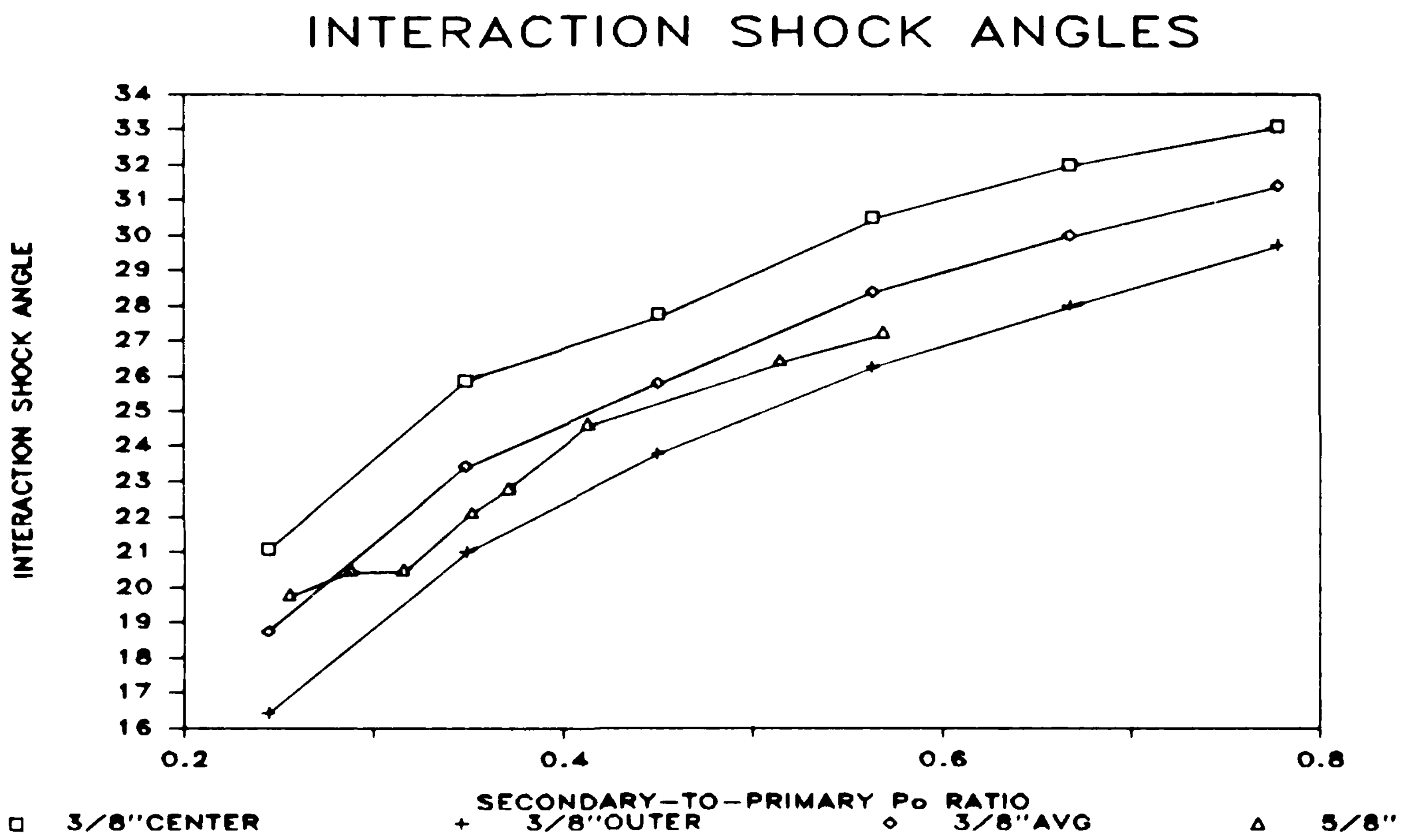

Figure 26. Interaction Shock Angles for Test Sections #2 and #3

reservoir pressure ratio. The average angles for both test sections agreed to within about one degree. Shock angles for test section #3 measured less because of the greater upstream Mach number. However, an interesting result was discovered in test section #2. The interaction shock angle was consistently about four degrees larger across the center nozzle than across the primary nozzles. For test section #3, with its deeper test cavity, the interaction shock angles for the center nozzle were larger by only a small amount, that could not be consistently measured so a single value was obtained. This value is plotted to compare with the average interaction shock angle of test section #2.

The difference in angle can be explained by a difference in geometry on the convergent side of the nozzles. The approach to the center primary nozzle was different than that to the outer primary nozzles. The outer nozzles ingest the boundary layer on the upper and lower walls approaching the half nozzle blocks, and had a smaller convergent area. These differences combine with thickening sidewall boundary layers, to decrease mass flow through the outer primary nozzles. The actual total pressures measured for test section #2, shown in Table 5, and for test section #3, shown in Table 6, confirm that less total pressure was lost by the air flowing through the center nozzle. This may explain the difference in shock interaction angles between the center and outer primary nozzles.

Other Boundary Layer Effects

Viscous effects also influenced static pressure measurement just downstream of the nozzle. As seen in Figure 16, for test section #2, which was most influenced by boundary layers, the pressure remained relatively constant until about .200 inches before reaching the interaction shock, then rose to a maximum near the shock location. Expansion waves originating from the expansion around the end of the nozzle block caused static pressure to drop off again. The pressure remained relatively constant for a short distance and then began increasing before the reflected shock location.

The diffusion of the static pressure through the boundary layer was discussed earlier. A comparison of nozzle centerline static pressures for the two test section depths at similar reservoir pressures may be made by considering Figure 27, which is identical to Figure 16, and Figure 28. Pressures in the 5/8 inch deep test section rise and fall more dramatically with increasing axial location, but the pressure trends for the two test sections are similar.

In Figure 29 , three runs at the same reservoir pressure ratios are compared, two of which illustrate conditions in test section #3: the plus symbol represents

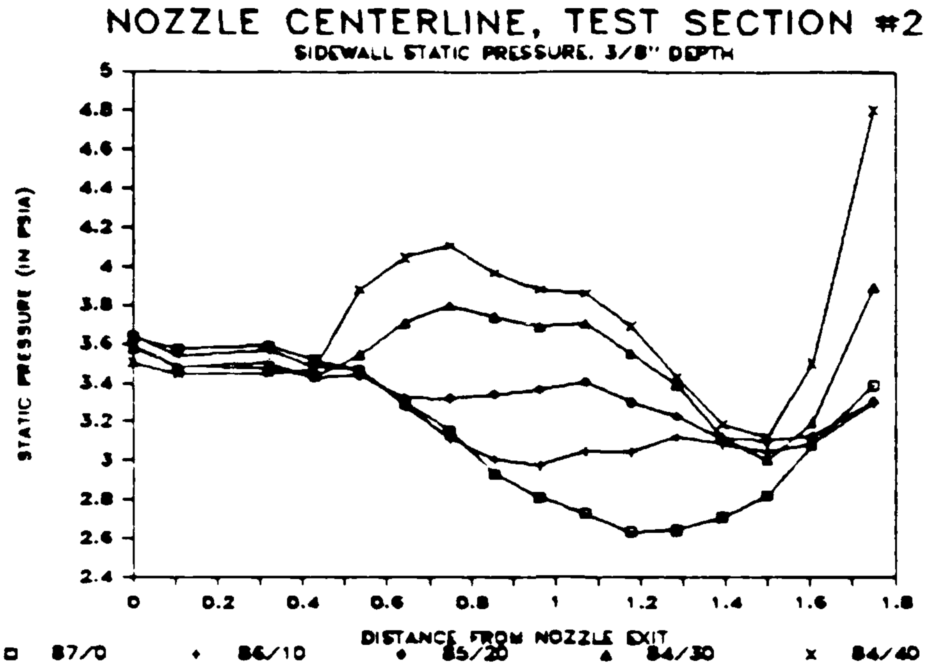

Figure 27. Test Section #2 Upper Centerline Static Pressures

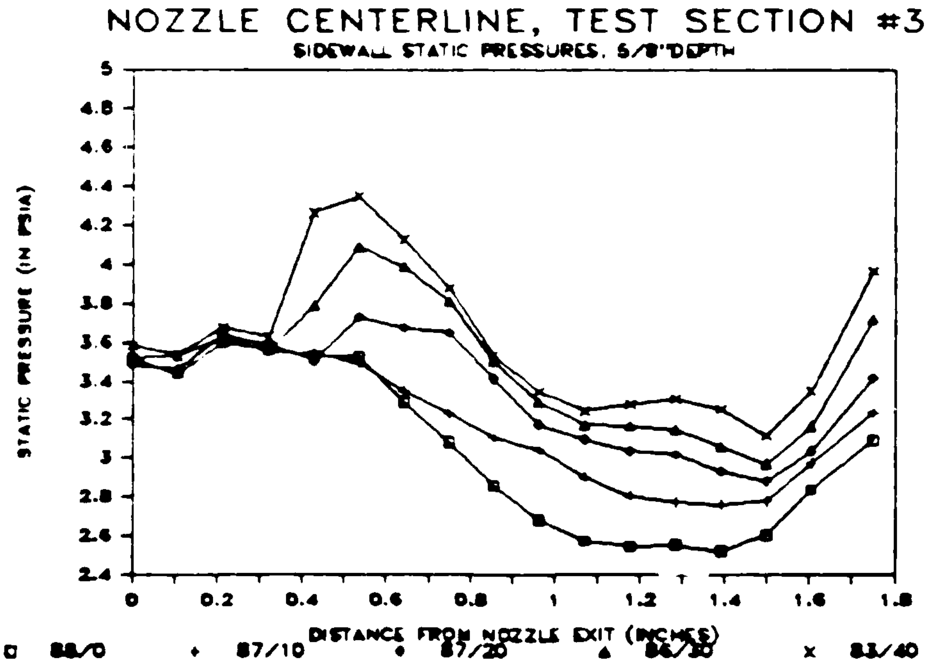

Figure 28. Test Section #3 Upper Centerline Static Pressures

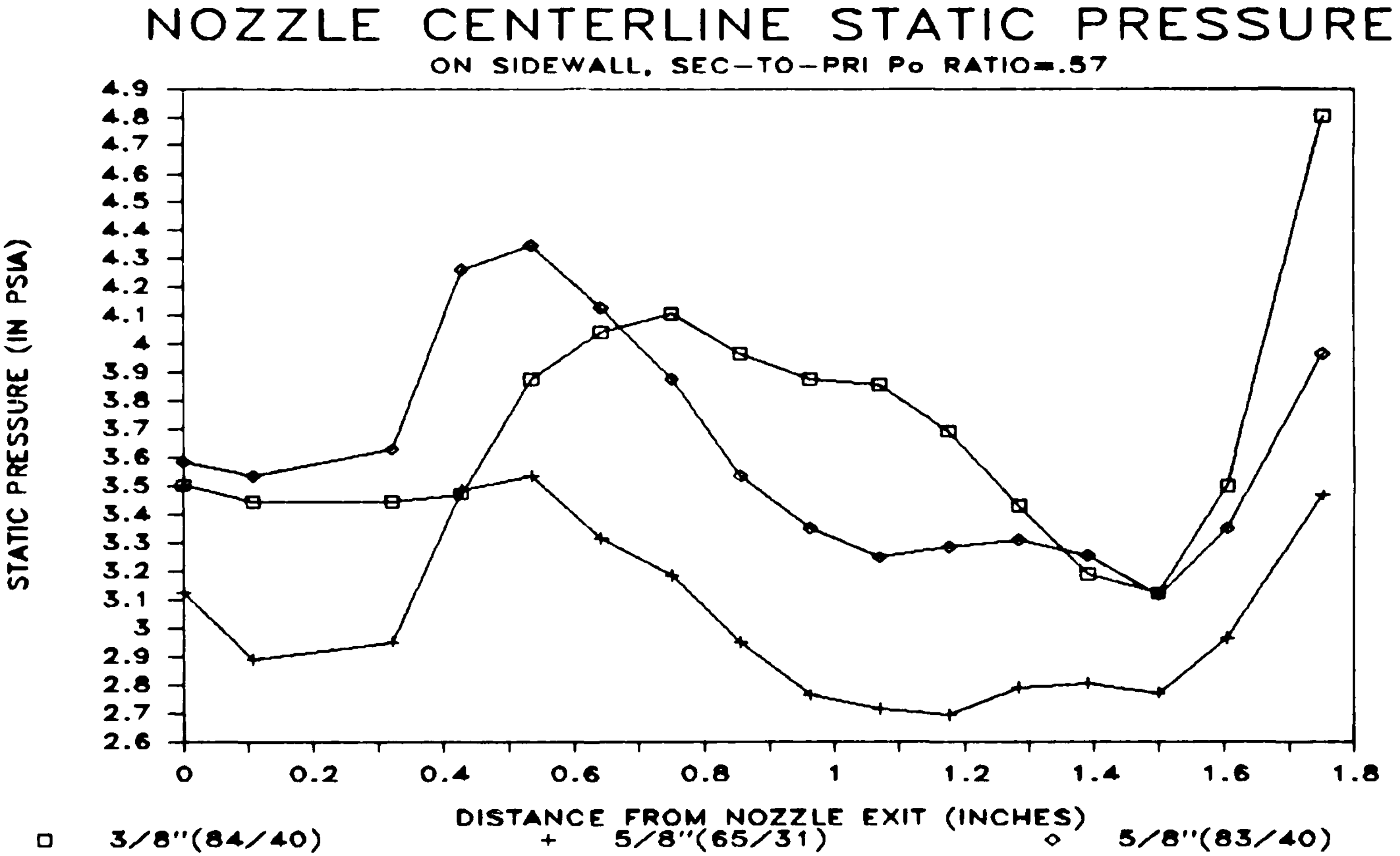

Figure 29. Comparison of Static Pressure In Test Sections #2 and #3 for the Same Secondary-to-Primary Reservoir Pressure Ratio.

flow at Po_s = 31 psig and Po_p = 65 psig; the diamond symbol represents flow at Po_s = 40 psig and Po_p = 83 psig. These are the same reservoir pressure ratios, but higher pressures cause higher mass flows in both nozzles for the diamond symbol. The curves are similar in shape, but one is displaced from the other due to a difference in total pressures. The curve from test section #2, 3/8 inch depth (square symbol), is much flatter due to boundary layer displacement and diffusion through the boundary layer at shock locations. If there are no losses, or the losses are linear the two curves for test section #3, 5/8 inch depth, should become one by multiplying by the ratio of reservoir pressures. This is done in Figure 30 and the curves superimpose, except at the nozzle exit and at the end. The downstream loss can be explained by higher frictional losses in the higher pressure flow because friction is proportional to the density of the flow.

Momentum Deficit in Wake of Sonic Nozzle

A momentum deficit exists in the wake of the nozzle block, due to lower velocity in the secondary flow compared to the primary flow. This can enhance mixing in a supersonic flow. The centerline Mach number of the center and outer primary nozzles and the sonic nozzle streams are plotted in Figure 31 for test section #3 with $Po_s/Po_p = 0.43$.

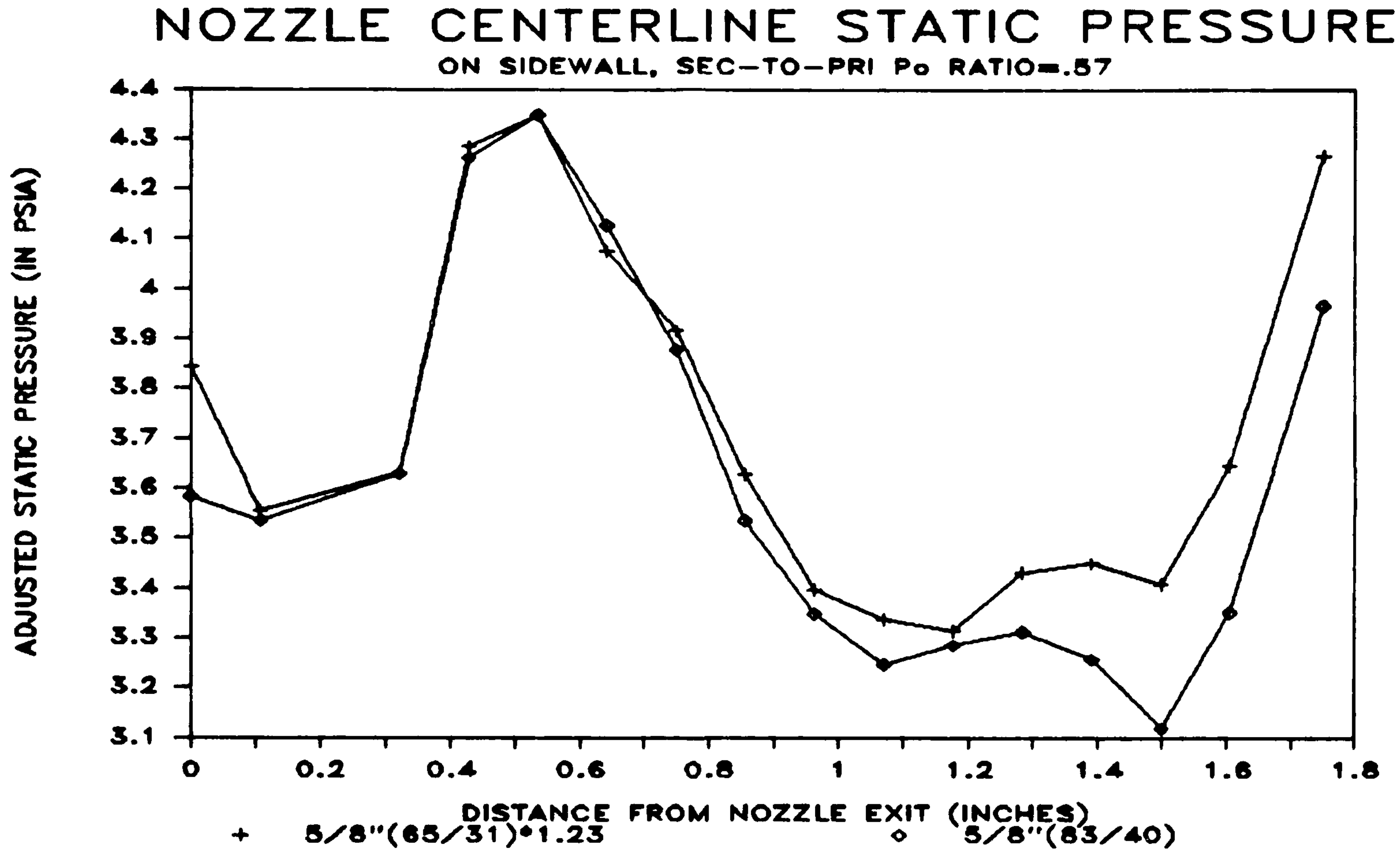

Figure 30. Similarity of Static Pressure at Same Reservoir Pressure Ratio Adjusted for Total Pressure Difference.

The one dimensional model predicts Mach numbers of the primary and secondary streams, to be 3.06 and 2.5 respectively. The one dimensional analysis was adjusted for known primary exit conditions of Mach = 2.8, instead of 3.0, and a total pressure loss of 8%. This analysis, presented in Table 2, predicts primary and secondary nozzle Mach numbers of 2.89 and 2.34. The actual secondary Mach is well below the predicted value. Therefore, the velocity difference between primary and secondary flows is greater than predicted. This is because expansion and friction losses in the secondary stream are not included in the analysis. Since the one dimensional analysis underpredicts the momentum differential as indicated by Mach number difference, it would also underpredict mixing.

The momentum differential decreases as reservoir pressure ratio increases, as seen in Figure 32. In this instance, the adjusted one dimensional analysis predicts primary and secondary Mach numbers of 2.85 and 2.5. The observed values near the nozzle are below that predicted, but do increase with increasing sonic reservoir pressure.

The effect of the momentum deficit is observed in the schlieren photographs as turbulence created by the shear layer downstream of the sonic nozzle. As seen in Figure 18, the turbulence in the shear layer between the secondary and primary flow streams becomes less apparent

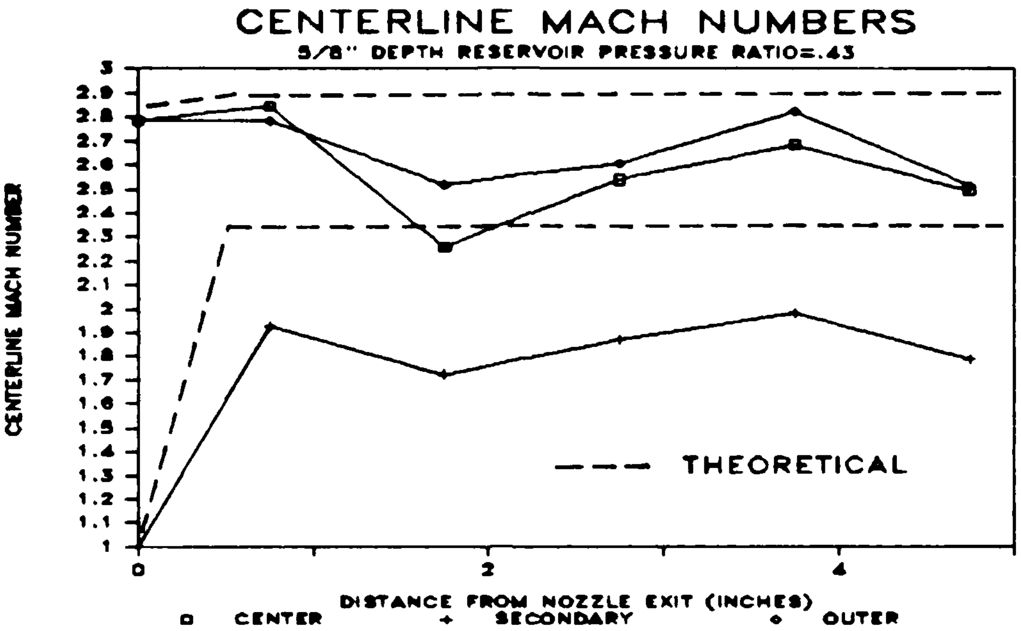

Figure 31. Nozzle Centerline Mach Number with Weaker Shock, Measured in Test Section #3 vs. Adjusted Theoretical

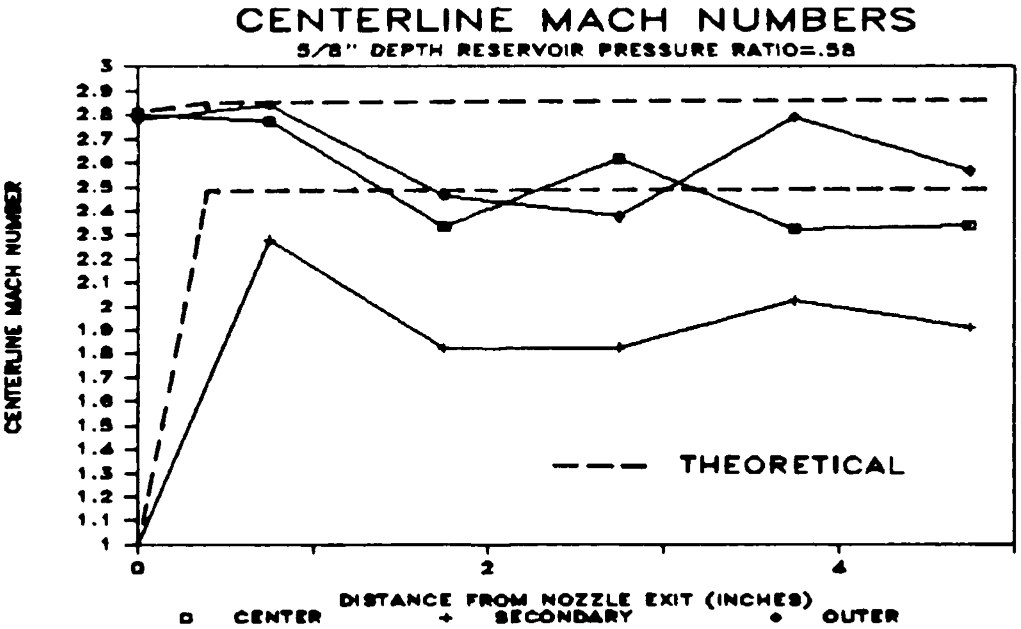

Figure 32. Nozzle Centerline Mach Number with Stronger Shock, Measured in Test Section #3 vs. Adjusted Theoretical

Table 2

ONE DIMESIONAL ANALYSIS OF TEST SECTION #3 FOR MEASURED NOZZLE EXIT CONDITIONS OF MACH=2.8 INCLUDING A TOTAL PRESSURE LOSS OF 8%

GAMMA 1.4

	SECONDARY			PRIMARY		
PoS/ PoP	MACH	A/A*	P/Po	MACH	A/A*	P/Po
0.05	1.008	1.000	.52343	3.026	4.342	.02617
0.10	1.509	1.182	.26892	3.008	4.268	.02689
0.15	1.759	1.396	.18521	2.986	4.180	.02778
0.20	1.927	1.589	.14315	2.966	4.102	.02863
0.25	2.053	1.764	.11774	2.948	4.030	.02943
0.30	2.153	1.924	.10067	2.931	3.965	.03020
0.35	2.236	2.070	.08840	2.915	3.905	.03094
0.40	2.307	2.207	.07913	2.900	3.850	.03165
0.45	2.368	2.334	.07188	2.886	3.798	.03235
0.50	2.423	2.454	.06603	2.872	3.749	.03302
0.55	2.471	2.566	.06122	2.859	3.703	.03367
0.60	2.515	2.673	.05719	2.847	3.659	.03431
0.65	2.555	2.775	.05377	2.835	3.618	.03495
0.70	2.591	2.872	.05081	2.823	3.578	.03557
0.75	2.625	2.964	.04823	2.812	3.541	.03617
0.80	2.656	3.053	.04597	2.801	3.505	.03677
0.85	2.685	3.137	.04396	2.791	3.470	.03736
0.90	2.712	3.220	.04217	2.781	3.436	.03795
0.95	2.737	3.298	.04056	2.771	3.404	.03853
1.00	2.761	3.374	.03910	2.761	3.373	.03910

as secondary reservoir pressure increases. The increased velocity of the secondary flow stream decreases the velocity differential between the streams and the apparent turbulence intensity. The mixing decreases as turbulence decreases according to the Prandtl energy method for jet mixing (20:1270).

Average Flow Conditions In Test Section

The average properties at one cross section in the duct were approximated by averaging the nine values measured at that cross section. Since the 5/8 inch deep test section was less affected by boundary layers, the average values of static pressure, total pressure, and Mach number were computed for three flow conditions in test section #3, 5/8 inch depth. The results are presented in Figures 33-35. The averages at the first two locations behind the nozzle are unreliable due to strong shocks near these locations. The averages at the nozzle and the last measurement location, 4.75 inches downstream of the nozzle exit, were used as a measure of overall performance.

The difference in measured average downstream properties for increasing shock strength was not great. Shock strength increased with an increase in secondary reservoir pressure, Po_s, due to greater turning of the primary flow. The nozzle exit Mach number of 2.8 decreased to 2.4 at the last location, 4.75 inches behind

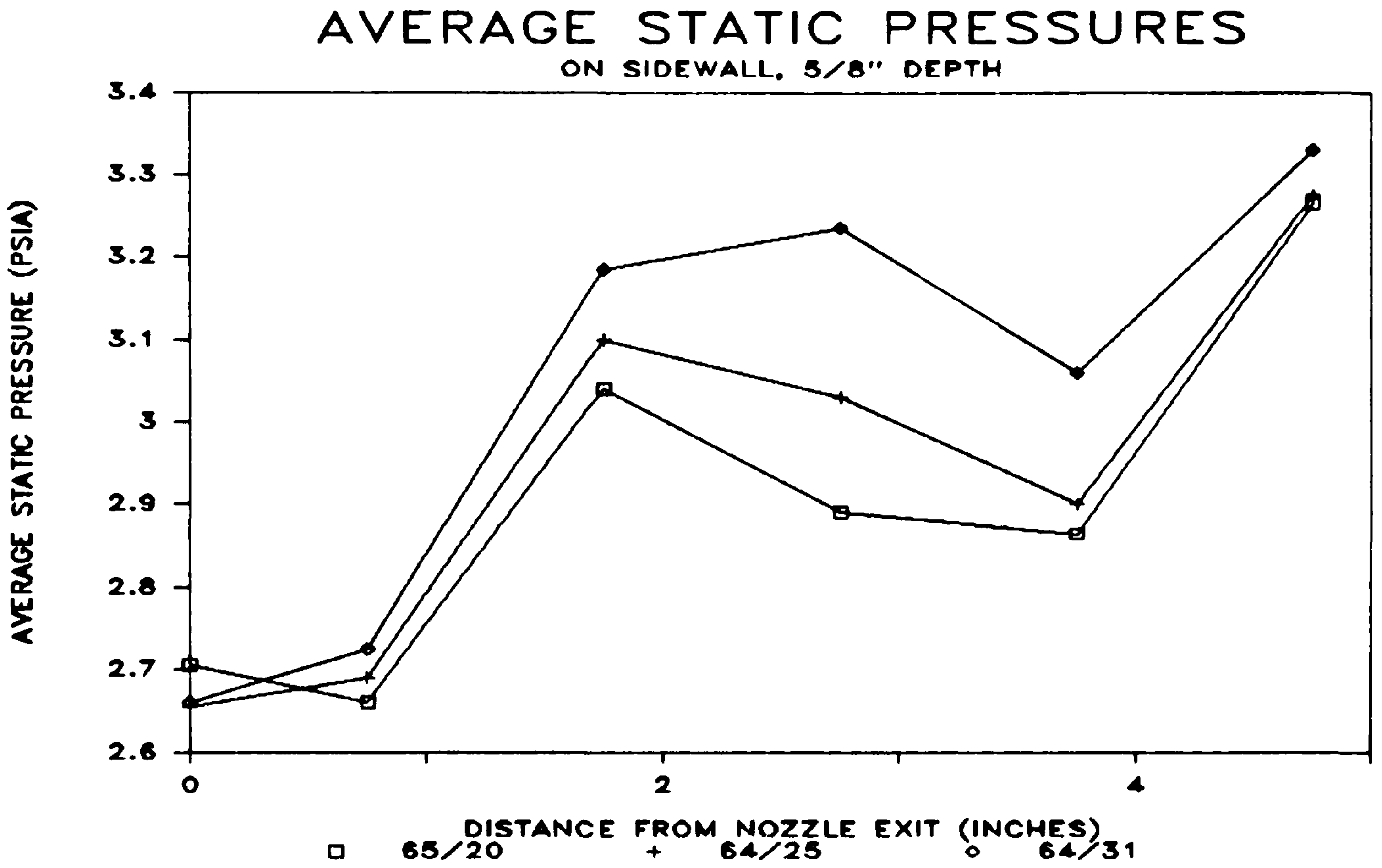

Figure 33. Average Static Pressures for Test Section #3

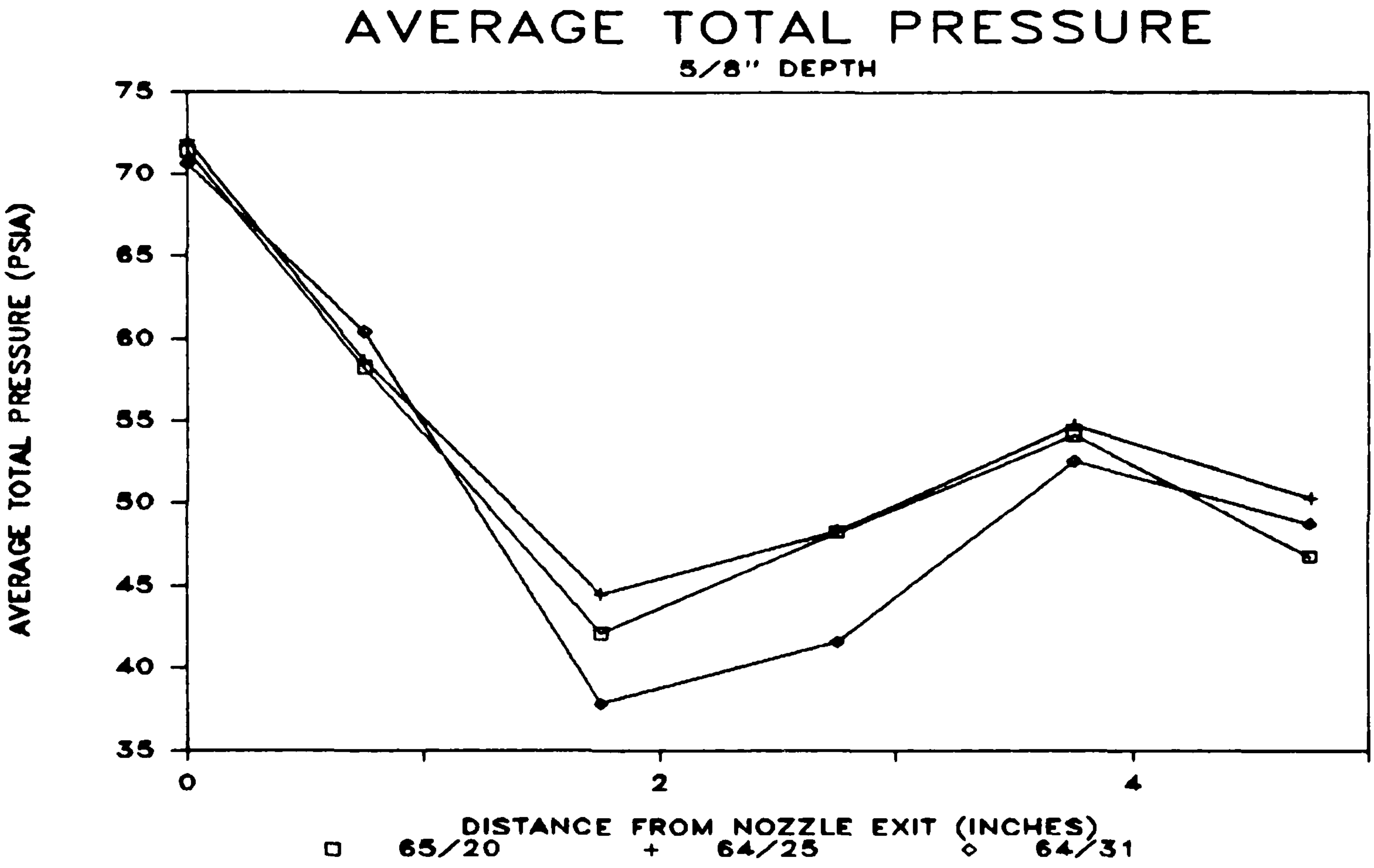

Figure 34. Average Total Pressures for Test Section #3

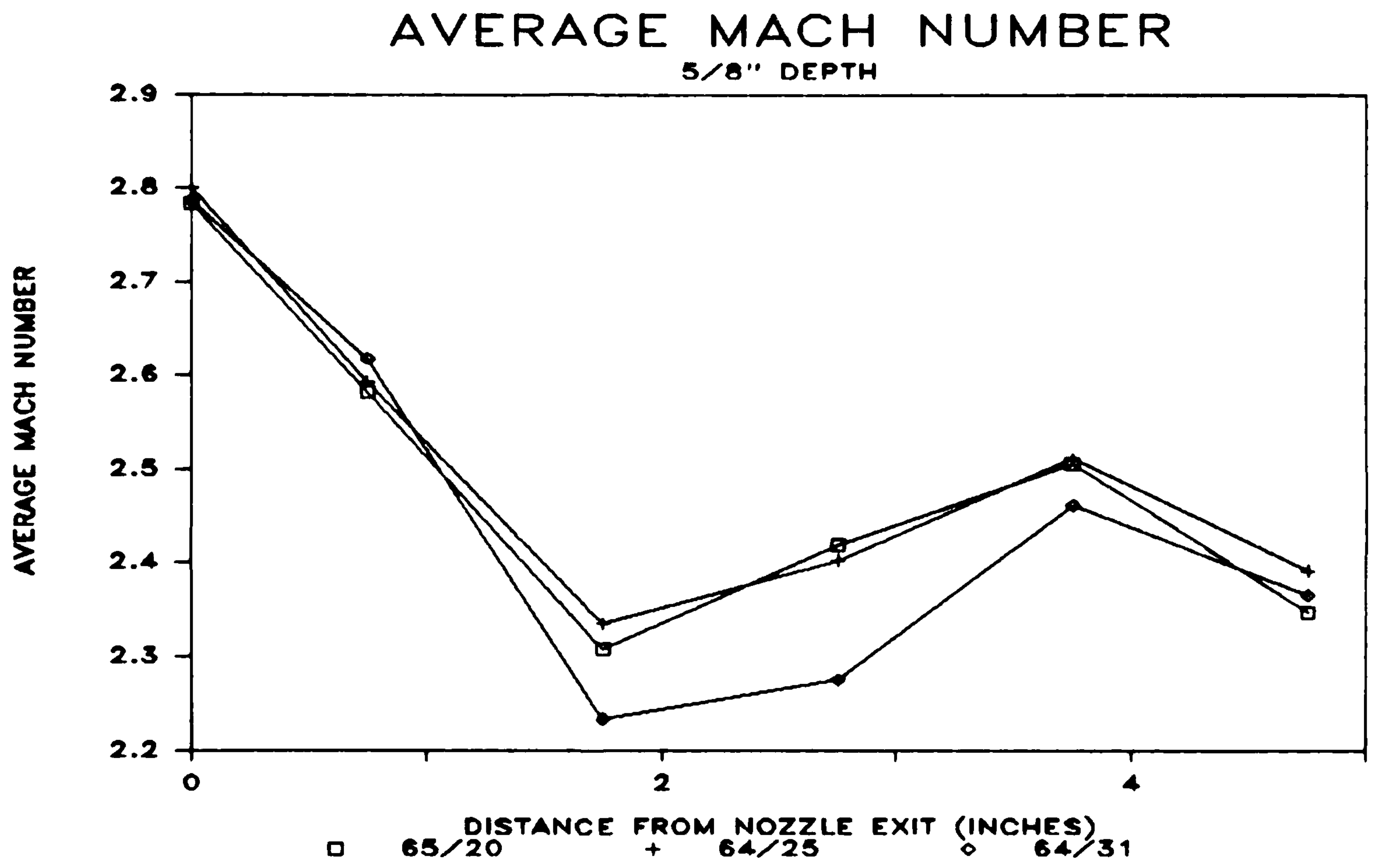

Figure 35. Average Mach Number for Test Section #3

the nozzle exit. For comparison, a single oblique shock with a turning angle of eight degrees would produce this Mach number change. In Table 3, the measured properties at the last measurement location are compared with properties calculated for an oblique shock, and properties calculated for one-dimensional, Fanno, frictional flow.

TABLE 3

Comparison of Friction and Oblique Shocks to Cause Measured Properties

	Measured Nozzle Properties	Oblique Shock	Fanno Friction	Measured (4.75") Properties
Mach	2.8	2.4	2.4	2.4
Total Pressure (psia)	72	70	49	48
Static Pressure (psia)	2.7	4.73	3.44	3.2

The comparison in Table 3 leads to the conclusion that the average performance of flow downstream of the nozzle in the 5/8" test section may be modeled with frictional, rather than shock effects.

Test Section #4 - Heat Addition by Combustion

A flame will blow off a burner in high speed flow. However, low velocities in the wake of a bluff body will create a small region where a stable flame may be held.

Pressures were measured in test section #4, with no flame, using the 8.5 inch plexiglass sidewalls. The diffuser was used on the end of the test section. The blunt end of the centerbody between the two nozzles created a recirculation region that extended at least one inch beyond the nozzle exit. This can be seen in the left center of Figure 36 from the blunt end of the centerbody to the point where the wake begins to widen behind the recompression shock. The recompression shocks curve back to the upper and lower walls. Turbulence in the wake is overcoming the momentum deficit, accelerating the flow in the wake.

No pressure measurements were made in the test section with the 2.75 inch long plexiglass sidewalls. However, schlieren photography was used to observe the flow. It is obvious in Figure 37 that the air flow could not overcome the wake region in this short test section configuration, with no diffuser. The flow became subsonic before reaching the end of the windows. The same flow was seen in the test section with the quartz windows, Figure 38. The flow beyond the windows was turbulent with no obvious structure.

The final portion of this investigation was a demonstration of combustion in the test section. Figure 39 pictures the combustion of premixed oxygen and acetylene with no air flow. As air flow increases, the air nozzles "start" and the flame is confined to the recirculation zone. In a schlieren picture, Figure 40,

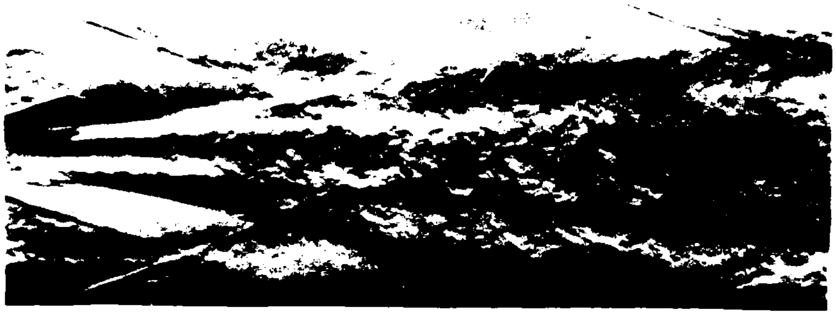

Figure 36. Cold Flow in Test Section #4 with Long Plexiglass Sidewall, Po= 84 psig

Figure 37. Cold Flow in Test Section #4 with Short Plexiglass Sidewall, Same Length as Combustion Model

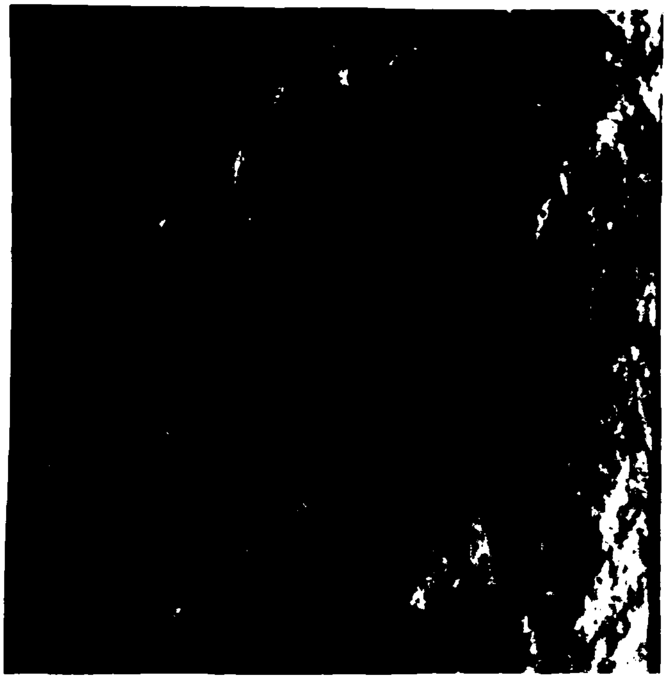

Figure 38. Flow in Free Area Beyond Windows with No Flame Test Section #4

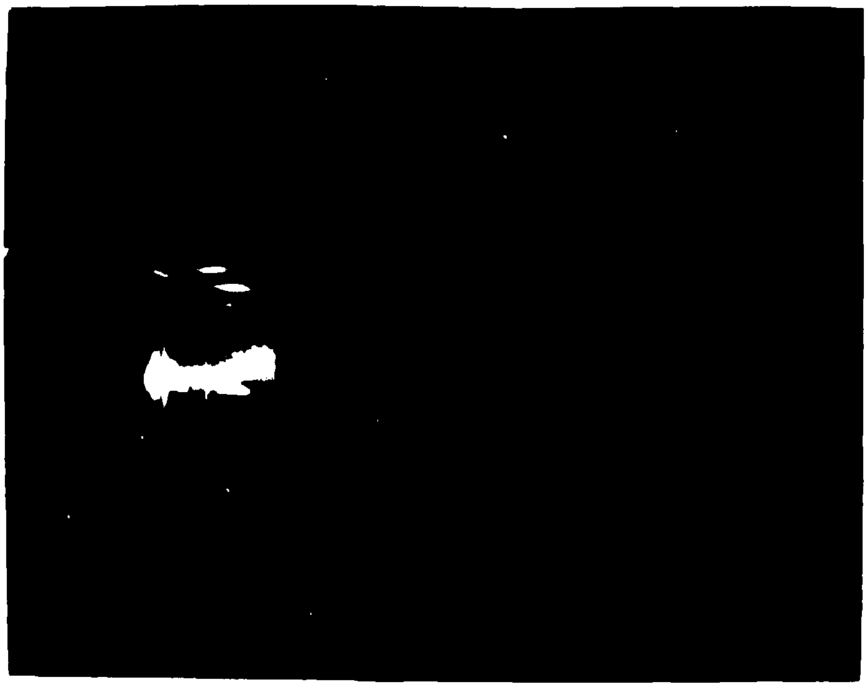

Figure 39. Picture of Flame in Test Section #4 with No Air Flow

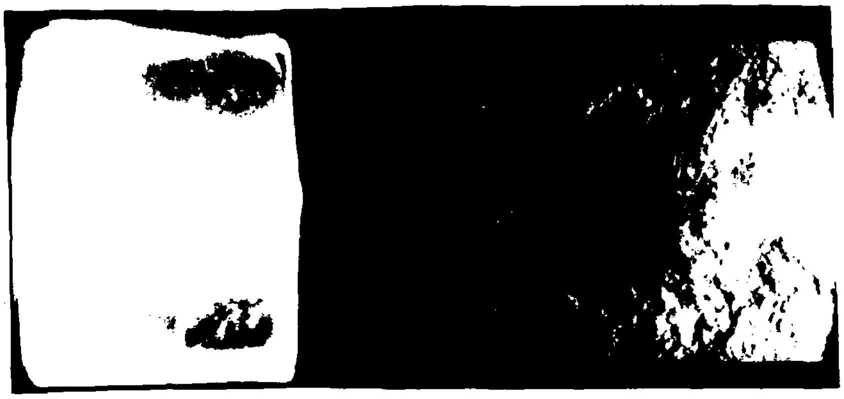

Figure 40. Schlieren of Test Section #4 with Combustion Heat Addition

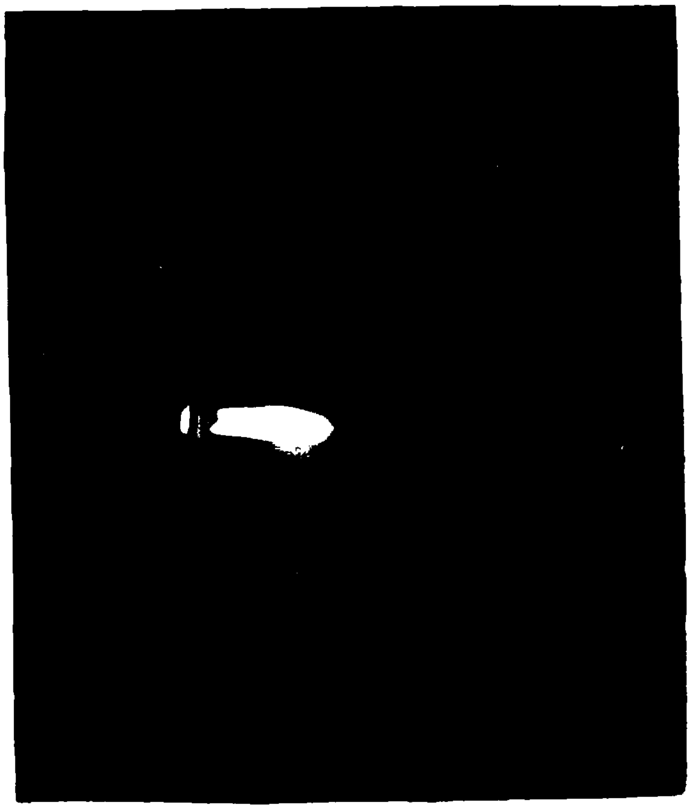

Figure 41. Picture of Oxygen [illegible]

AD-A189 572 INTERACTION BETWEEN TWO-DIMENSIONAL SONIC JETS AND SUPERSONIC FLOW TO MOD (U) AIR FORCE INST OF TECH WRIGHT-PATTERSON AFB OH SCHOOL OF ENGI J M TRAXLER 2/2

UNCLASSIFIED DEC 87 AFIT/GA/AA/87D-07 F/G 21/2 NL

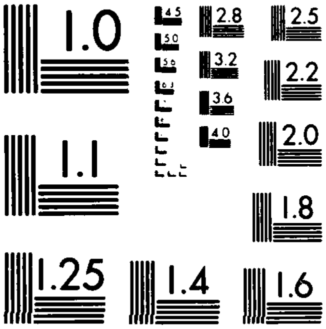
1.0
1.1
1.25
1.4
1.6
1.8
2.0
2.2
2.5
2.8
3.2
3.6
4.0
4.5
5.0
5.6
6.3

MICROCOPY RESOLUTION TEST CHART
NATIONAL BUREAU OF STANDARDS-1963-A

the luminous flame obscured detail of the flow around the flame. No shocks can be seen. However, the flow in the free region beyond the window frame now is organized into three separate non-spreading jets.

An oxygen rich flame is pictured in Figure 41. When this flame was observed directly, the luminous gases leaving the flame near the nozzle were drawn back toward the nozzle. The "corona" of luminous gases around the flame was about twice the height of the end of the centerbody. A slow circulation of the luminous gases in this region was observed. A possible explanation for this would be that heat addition has increased the base pressure well above the design nozzle exit static pressure. This caused boundary layer separation inside the nozzle creating a shock, as depicted in Figure 42. The luminous gases were observed recirculating into the separated flow region in the nozzle. Fuel was cut off at the end of the run. An increase in noise level was noted as the flow returned to its chaotic state.

This investigation explored two extremes of the heat addition problem. Never, in the mass addition investigation, was enough mass added to raise the base pressure above the nozzle exit static pressure, or to choke the flow in the constant area duct. On the other hand, in the hot flow demonstration the amount of heat added caused flow separation of inside the primary nozzles.

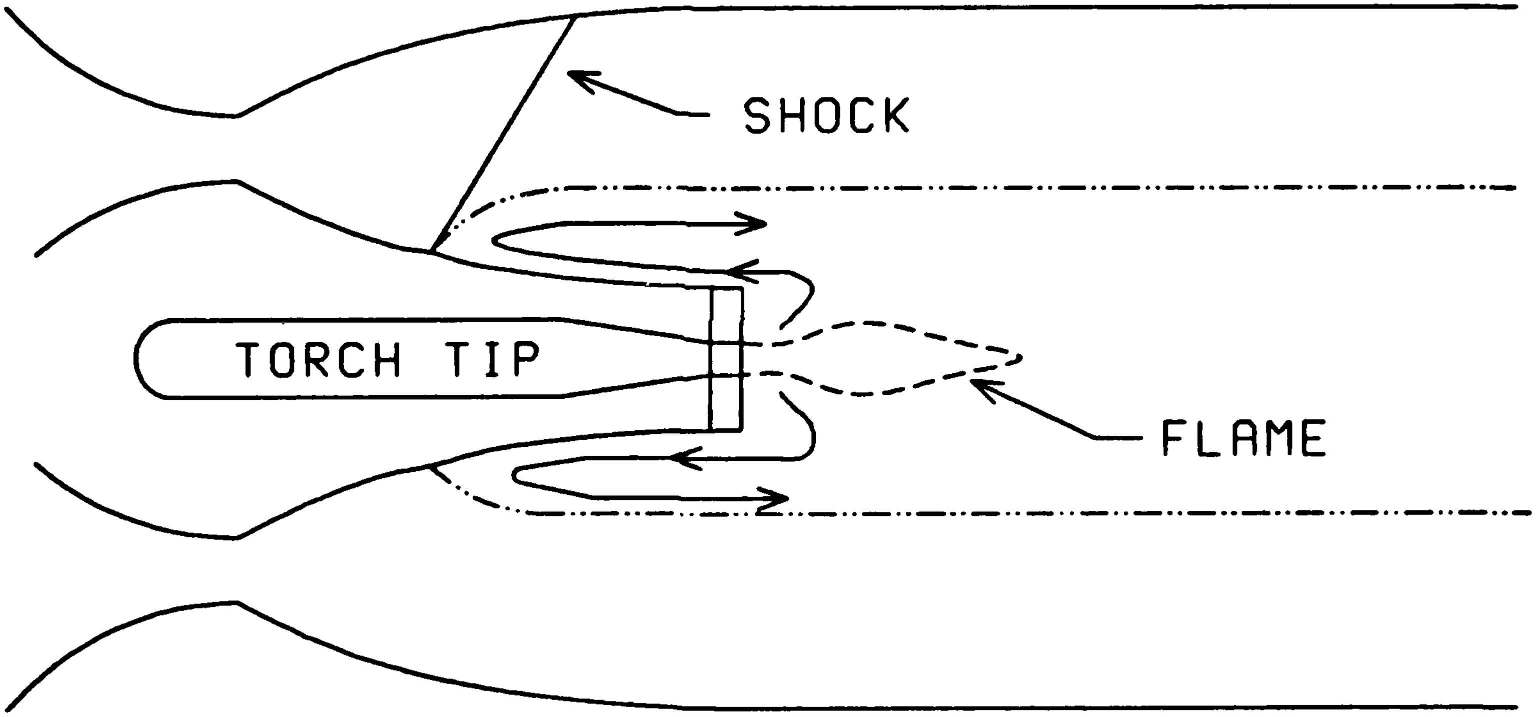
SHOCK
TORCH TIP
FLAME

Figure 42. Schematic of Flow in Test Section #4 with Heat Addition

VI. Conclusions and Recommendations

Conclusions

This investigation used the equivalent displacement of mass addition to model heat addition in a supersonic flow. Four different test sections were used in this investigation.

Off-design nozzles increase turbulence and could be used as a method to enhance mixing. However, such a configuration is not efficient and produces large total pressure losses. Pressure measurement near the nozzle is difficult and of questionable accuracy because of expansion waves from the nozzle.

Sidewall static pressure measurements in the vicinity of strong shocks are not equal to the static pressure in the center of the two-dimensional test cavity because of pressure diffusion through the boundary layer. This made analysis of the flow field difficult, however understanding of the problem was aided by an optical study, and a few simple models of the problem.

The structure of the precombustion shock zone, as determined by the mass addition investigation, is primarily a base flow problem, which is somewhat dependent on turbulence intensity. A simple one dimensional isentropic expansion model gave a reasonable estimate of stream properties that were confirmed by experimental data. Although it is theoretically possible to model "thermal compression" with an expanding sonic jet, the results of this investigation were dominated by frictional effects due to the scale of the test equipment. Therefore, it is necessary to include frictional effects in high speed, high temperature flow analysis.

It is possible to burn a premixed oxygen- acetylene mixture injected in the base region behind a blunt end between two supersonic nozzles. The amount of heat added in this investigation combined with the external ambient pressure to cause flow separation in the primary nozzles.

Recommendations

It was not possible to see the effects of shock-boundary layer interaction on the sidewall. Investigation into the process of diffusion through the boundary layer would support later investigations in which shocks may affect sidewall static pressure readings.

The base flow problem with a sonic flow through the base region and the effect of approaching boundary layer must be understood to control mixing in a supersonic flow. A test section of sufficient scale with a means of boundary layer control would be necessary to study this problem.

The investigation of heat addition to a supersonic flow must continue. The reason the area of the hot jet is greater than the end of the centerbody must be known. The low enthalpy combustion is a problem. It is still unknown if there is an upper and lower limit on how much heat can be added in the recirculation region and the stability limits of the flame.

Bibliography

1. Billig, F.S. "Combustion Processes in Supersonic Flow," Notes from the Johns Hopkins University Applied Physics Laboratory, Silver Springs, Maryland. Lecture at the Seventh International Symposium on Air Breathing Engines.

2. Billig, F.S. and others. "Effects of Thermal Compression on the Performance Estimates on Hypersonic Ramjets," Journal of Spacecraft and Rockets: 1076-1081, Vol.5, No.9 (Sept.1968).

3. Billig, Frederick S. "Hydrocarbon, High Energy and Reactive Fuels for Supersonic Combustion Engines." Notes for lecture given at the University of Tennessee Space Institute at Arnold AFS, Tullahoma, Tennessee, July 12-23, 1965.

4. Billig, F.S. and others. "Integral-Rocket Dual-Combustion Ramjets: A New Propulsion Concept," Journal of Spacecraft and Rockets: 416-424, Vol.17, No.5 (Sept-Oct 1980).

5. Billig, F.S. "Two-Dimensional Model for Thermal Compression," Journal of Spacecraft and Rockets: 702-703, Vol.9, No.9 (September 1972).

6. Billig, F.S. and G.L. Dugger. "The Interaction of Shock Waves and Heat Addition In the Design of Supersonic Combustors," Twelfth Symposium International on Combustion: 1125-1139. Pittsburg: The Combustion Institute, 1969.

7. Bonney, Capt. Roy L. Two Dimensional Supersonic Jet Mixing of Air and Helium. M.S. thesis, AFIT/GAE/AA/78D-2. School of Engineering, Air Force Institute of Technology (AU), Wright-Patterson Air Force Base OH, December 1978.

8. Carlile, Capt. John D. Design and Evaluation of a Facility To Study Two-Dimensional Supersonic Air-Helium-Mixing. M.S. thesis, AFIT/GAE/AA/78M-4. School of Engineering, Air Force Institute of Technology (AU), Wright-Patterson AFB OH, March 1978.

9. Chapman, Dean R. "An Analysis of Base Pressure at Supersonic Velocities and Comparison with Experiment," N.A.C.A. Technical Note 2137. Washington: 1950.

10. Chow, W.L. "On the Base Pressure Resulting From the Interaction of a Supersonic External Stream With a Sonic or Subsonic Jet," Journal of the Aerospace Sciences: 176-180 (March 1959).

11. Crocco, Luigi and Lester Lees. "A Mixing Theory for the Interaction Between Dissipative Flows and Nearly Isentropic Streams," Journal of the Aeronautical Sciences: 649-676 Vol.19 No.10 (October 1952).

12. Drummond, J. Phillip and Elizabeth H. Weidner. "Numerical Study of a Scramjet Engine Flowfield," AIAA Journal. 1182-1187 Vol.20 No.9 (September 1982).

13. Ferri, Antonio. "Supersonic Combustion Progress," Astronautics and Aeronautics: 32-37 (August 1964).

14. Korst, H.H. "A Theory for Base Pressures in Transonic and Supersonic Flow," Journal of Applied Mechanics: 593-599 (December 1956).

15. Kumar, Ajay and others. AIAA-87-1882, A Mixing Augmentation Technique for Hypersonic Scramjets: AIAA/SAE/ASME/ASEE 23rd Joint Propulsion Conference, San Diego, June 29-July 2 1987.

16. Nash, John F. An Analysis of Two-Dimensional Turbulent Base Flow, Including the Effect of Approaching Boundary Layer: Ministry of Aviation, Aeronautical Research Council, Reports and Memoranda No. 3344. London, July 1962.

17. Northam, G. Burton and G. Y. Anderson. AIAA-86-0159, Supersonic Combustion Ramjet Research at Langley: AIAA 24th Aerospace Sciences Meeting, Reno, Nevada, January 6-9 1986.

18. Rues, D. Concerning the Equivalence Between Heat-, Force-, and Mass-Sources: Ministry of Aviation, Library Translation No. 1119 of Report From Institut Fur Theoretische Gasdynamik der Deutschen Versuchsanstalt Fur Luft-und Raumfahrt e.V. (D.V.L.)Aachen. Farnborough Hants, July 1965.

19. Rubins, P.M. and T.H.M. Cunningham. "Shock Induced Supersonic Combustion in a Constant-Area Duct," Journal of Spacecraft and Rockets: 199-205, Vol.2, No.2 (March-April 1965).

20. Schetz, J.A. and others. "Flowfield Analysis of a Scramjet Combustor with a Coaxial Fuel Jet," AIAA Journal: 1268-1274, Vol.20 No.9 (Sept. 1982).

21. Schlichting, Hermann. Boundary-Layer Theory (Seventh Edition). New York: McGraw-Hill Book Company, 1979.

22. Shapiro, Ascher H. The Dynamics and Thermodynamics of Compressible Fluid Flow, Volume I. New York: Wiley and Sons, 1953.

23. Shapiro, Ascher H. The Dynamics and Thermodynamics of Compressible Fluid Flow, Volume II. Malabar, Florida: Robert E. Krieger Publishing Company, Reprint 1985.

24. Speir, Capt. Ross C. A Theoretical Investigation on the Effect of Mixing on Thermal Choking in Scramjet Combustors. M.S. thesis, AFIT/GAE/AE/75M-4. School of Engineering, Air Force Institute of Technology (AU), Wright-Patterson AFB OH, March 1975.

25. Stull, Frank D. "Scramjet Combustion Prospects," Astronautics and Aeronautics: 48-52 (December 1965).

26. Waltrup, P.J. and F.S. Billig. "Structure of Shock Waves in Cylinderical Ducts," AIAA Journal: 1404-1408, Vol.11 No.10 (October 1973).

27. Watton, Alan Jr. The Mechanism of the Fuel-Mixing Process Diffusion-Type Supersonic Combustion. ASD-TR-68-62. Wright-Patterson Air Force Base, Ohio: Aeronautical Systems Division, Air Force Systems Command, September 1968.

28. Wilder, John G. and Kenneth Hindersinn. "Spreading of Supersonic Jets in Supersonic Streams," Aeronautical Engineering Review: 54-68 (October 1953).

29. Zierep, J. Theory of Flows in Compressible Media with Heat Addition. AGARDograph No. 191. North Atlantic Treaty Organization Advisory Group for Aerospace Research and Development.

APPENDIX A: SELECTED DATA SETS FOR TEST SECTIONS #1-#3

Table 4

Data Set, Test Section #1

```
          ATMOSPHERIC PRESSURE = 14.3154 in PSI
          PRIMARY GAGE PRESSURE 84
          SECONDARY GAGE PRESSURE 40
                                      PORTS 1 THROUGH 9
          ROW                      STATIC PRESSURE IN PSIA

1.00       3.48     2.61     2.46     3.24     5.14     2.66     2.24     2.32     4.18
2.00       4.22     3.57     3.32     2.88     2.56     2.93     3.75     5.44     5.64
3.00       3.51     3.41     3.41     4.30     4.38     4.63     3.43     3.34     3.52
4.00       3.28     5.18     4.42     4.36     4.45     4.45     4.80     4.31     3.65
5.00       3.84     3.93     4.05     4.83     5.08     4.24     4.23     4.21     4.00
          NOZZLE EXIT
          1        3.50
          2        3.86
          3        3.85

                                      PORTS 1 THROUGH 9
          ROW             MEASURED TOTAL PRESSURE IN PSIA

1.00      32.55    20.33    22.25    22.86    47.62    24.71    20.67    18.83    21.55
2.00      33.23    23.57    19.72    20.97    12.40    18.28    20.55    25.24    25.13
3.00      29.33    24.16    18.90    32.24    15.32    28.15    18.15    23.94    26.68
4.00      20.50    28.46    20.58    31.15    25.43    28.55    21.04    28.68    22.66
5.00      27.36    21.58    19.58    28.55    30.91    25.56    15.61    30.94    25.30
          NOZZLE EXIT
          1       34.04
          2       30.93
          3       29.39

                                      PORTS 1 THROUGH 9
          ROW               ACTUAL TOTAL PRESSURE IN PSIA

1.00      72.15    37.09    47.64    37.97   104.67    54.35    45.19    35.86    28.15
2.00      61.37    36.98    28.39    35.92    15.58    27.34    27.94    30.96    30.14
3.00      57.49    40.35    25.88    56.69    16.61    41.31    24.11    40.43    47.40
4.00      30.71    38.75    25.29    52.42    35.64    43.75    25.04    45.29    33.82
5.00      45.85    29.38    24.58    41.00    45.39    37.28    17.24    53.47    38.30
          NOZZLE EXIT
          1       79.03
          2       58.17
          3       52.63

                                      PORTS 1 THROUGH 9
          ROW                           MACH NUMBER

1.00       2.62     2.38     2.58     2.26     2.61     2.61     2.61     2.44     1.90
2.00       2.40     2.18     2.06     2.30     1.84     2.11     1.97     1.79     1.75
3.00       2.47     2.26     1.98     2.33     1.52     2.08     1.93     2.28     2.35
4.00       2.11     1.97     1.80     2.28     2.02     2.15     1.74     2.19     2.11
5.00       2.27     1.97     1.84     2.05     2.09     2.07     1.57     2.31     2.13
          NOZZLE EXIT
          1         2.68
          2         2.42
          3         2.36
```

Table 5

Data Set, Test Section #2

```
ATMOSPHERIC PRESSURE = 14.426 in PSI
PRIMARY GAGE PRESSURE 80
SECONDARY GAGE PRESSURE 40
                              PORTS 1 THROUGH 9
ROW                         STATIC PRESSURE IN PSIA

1.00    3.96    3.03    3.48    2.83    6.29    2.93    2.91    2.75    3.59
2.00    4.55    4.77    4.17    3.64    2.66    3.65    3.97    4.94    4.22
3.00    4.17    3.61    3.58    4.43    3.84    4.84    3.51    3.45    4.05
4.00    3.54    4.30    4.78    4.39    4.39    4.39    4.21    4.92    3.38
5.00    4.20    4.67    4.50    4.84    6.03    4.88    4.57    4.47    4.17
NOZZLE EXIT
1       3.46
2       3.65
3       3.64

                              PORTS 1 THROUGH 9
ROW               MEASURED TOTAL PRESSURE IN PSIA

1.00   39.35   27.63   22.93   21.93   48.47   24.95   20.30   27.13   40.29
2.00   37.54   28.50   22.31   31.30   20.32   29.35   21.83   30.05   32.80
3.00   21.04   19.99   16.52   20.43   18.10   22.21   17.84   18.23   19.93
4.00   17.04   24.95   13.81   21.01   21.60   22.93   15.18   23.62   16.38
5.00   22.78   26.66   16.40   18.57   24.45   25.53   17.38   14.89   15.88
NOZZLE EXIT
1     30.98
2     34.58
3     33.29

                              PORTS 1 THROUGH 9
ROW                 ACTUAL TOTAL PRESSURE IN PSIA

1.00   93.57   59.68   35.93   39.88   87.59   49.85   33.38   64.10  111.52
2.00   72.75   41.23   29.84   63.30   36.41   55.33   29.74   44.14   59.74
3.00   27.10   27.37   20.19   24.98   22.38   27.07   23.07   24.18   25.27
4.00   21.33   35.35   14.26   26.21   27.39   30.19   16.61   29.54   20.60
5.00   30.73   37.31   18.03   20.82   28.04   33.65   19.41   15.89   17.76
NOZZLE EXIT
1     65.38
2     77.83
3     72.06

                              PORTS 1 THROUGH 9
ROW                                MACH NUMBER

1.00    2.71    2.59    2.18    2.38    2.37    2.50    2.24    2.70    2.89
2.00    2.46    2.06    1.94    2.51    2.36    2.42    1.97    2.09    2.38
3.00    1.88    1.98    1.79    1.79    1.81    1.78    1.89    1.93    1.85
4.00    1.83    2.03    1.35    1.83    1.85    1.92    1.55    1.83    1.84
5.00    1.96    2.01    1.56    1.61    1.66    1.92    1.60    1.48    1.60
NOZZLE EXIT
1      2.56
2      2.64
3      2.59
```

Table 6

Data Set, Test Section #3

```
        ATMOSPHERIC PRESSURE = 14.316 in PSI
        PRIMARY GAGE PRESSURE 84
        SECONDARY GAGE PRESSURE 40
                                    PORTS 1 THROUGH 9
        ROW                      STATIC PRESSURE IN PSIA

1.00     3.97    2.80    3.37    2.70    5.03    2.46    2.84    2.72    3.66
2.00     4.23    4.54    4.46    3.53    2.63    3.45    4.28    4.52    3.89
3.00     4.30    4.03    3.56    3.60    3.23    4.11    4.06    3.99    3.96
4.00     3.31    3.77    3.59    4.12    4.60    4.28    3.56    3.64    3.19
5.00     4.09    4.55    4.66    4.18    3.27    4.16    4.56    4.32    3.82
        NOZZLE EXIT
        1       3.66
        2       3.34
        3       3.14

                                    PORTS 1 THROUGH 9
        ROW           MEASURED TOTAL PRESSURE IN PSIA

1.00    43.70   27.23   21.30   26.88   54.57   24.17   20.58   26.22   41.60
2.00    35.01   34.57   21.07   30.88   20.96   30.88   20.01   32.53   33.46
3.00    36.35   32.15   20.60   35.77   28.53   40.54   19.76   27.45   32.81
4.00    35.64   32.40   19.88   36.78   23.89   33.29   19.22   35.07   32.50
5.00    36.30   32.88   22.94   35.14   21.79   34.59   22.49   34.24   32.04
        NOZZLE EXIT
        1     35.91
        2     37.53
        3     34.38

                                    PORTS 1 THROUGH 9
        ROW             ACTUAL TOTAL PRESSURE IN PSIA

1.00 118.06    63.24   32.25   64.13  144.67   56.73   35.13   60.25  117.18
2.00   67.93   61.69   26.08   63.66   39.12   65.31   24.62   55.02   67.70
3.00   72.16   60.12   29.14   85.16   59.35   95.87   24.88   44.58   63.85
4.00   93.55   65.46   27.22   77.50   31.35   60.74   25.85   80.67   79.64
5.00   75.88   55.87   29.09   69.39   34.44   67.49   28.58   63.65   63.15
        NOZZLE EXIT
        1     84.39
        2    104.30
        3     92.23

                                    PORTS 1 THROUGH 9
        ROW                             MACH NUMBER

1.00     2.86    2.68    2.13    2.71    2.84    2.69    2.29    2.67    2.91
2.00     2.46    2.35    1.81    2.54    2.41    2.57    1.80    2.28    2.51
3.00     2.49    2.41    2.03    2.71    2.55    2.70    1.84    2.23    2.46
4.00     2.83    2.51    1.98    2.56    1.91    2.38    1.95    2.67    2.74
5.00     2.55    2.29    1.85    2.48    2.19    2.47    1.86    2.41    2.48
        NOZZLE EXIT
        1       2.69
        2       2.89
        3       2.85
```

Table 7

Data Set, Test Section #1 at Highest Secondary-to-Primary Reservoir Ratio Tested

ATMOSPHERIC PRESSURE = 14.425 in PSI
PRIMARY GAGE PRESSURE 79
SECONDARY GAGE PRESSURE 59

PORTS 1 THROUGH 9

ROW	STATIC PRESSURE IN PSIA								
1.00	4.46	3.27	2.46	4.05	8.13	4.14	2.07	3.05	3.72
2.00	6.10	4.93	4.06	3.06	2.06	3.24	3.93	6.07	5.90
3.00	5.62	4.06	3.95	4.07	4.09	4.50	3.93	3.99	5.48
4.00	4.04	3.76	6.41	5.71	5.11	5.35	5.59	4.39	3.96
5.00	4.44	4.88	4.88	5.88	6.03	5.93	4.84	4.65	4.45

NOZZLE EXIT
1 3.45
2 3.91
3 3.84

PORTS 1 THROUGH 9

ROW	MEASURED TOTAL PRESSURE IN PSIA								
1.00	38.45	23.97	27.55	24.21	41.25	32.47	25.81	25.28	39.00
2.00	47.95	29.75	26.39	31.26	18.87	29.28	26.51	32.92	47.29
3.00	43.54	29.33	24.20	37.92	25.86	37.67	24.27	28.67	41.60
4.00	33.15	32.40	28.94	36.63	23.65	35.08	30.30	35.27	32.68
5.00	34.21	37.83	26.51	38.08	25.24	34.15	27.71	34.36	35.62

NOZZLE EXIT
1 33.20
2 35.19
3 33.89

PORTS 1 THROUGH 9

ROW	ACTUAL TOTAL PRESSURE IN PSIA								
1.00	78.03	41.24	75.97	35.06	53.29	59.68	82.00	49.11	99.03
2.00	88.40	43.41	40.86	77.01	40.96	62.41	42.35	44.46	88.91
3.00	79.03	49.80	35.69	83.80	39.11	74.11	36.04	48.51	74.06
4.00	63.79	65.68	34.97	56.11	28.95	54.74	40.89	66.44	63.28
5.00	61.81	68.80	35.81	58.78	29.37	48.13	38.86	59.64	66.87

NOZZLE EXIT
1 76.17
2 74.83
3 70.46

PORTS 1 THROUGH 9

ROW	MACH NUMBER								
1.00	2.52	2.30	2.88	2.06	1.89	2.39	3.05	2.46	2.79
2.00	2.39	2.08	2.16	2.75	2.60	2.58	2.20	1.96	2.42
3.00	2.37	2.29	2.09	2.62	2.13	2.48	2.10	2.28	2.35
4.00	2.45	2.51	1.77	2.15	1.79	2.17	1.96	2.42	2.46
5.00	2.37	2.38	1.96	2.16	1.69	2.02	2.02	2.32	2.42

NOZZLE EXIT
1 2.67
2 2.57
3 2.55

Table 8

Data Set, Test Section #2 at Highest Secondary-to-Primary Reservoir Ratio Tested

```
        ATMOSPHERIC PRESSURE = 14.225 in PSI
        PRIMARY GAGE PRESSURE 82
        SECONDARY GAGE PRESSURE 57
                                     PORTS 1 THROUGH 9
        ROW                     STATIC PRESSURE IN PSIA

1.00     4.79    2.31    2.55    3.37    7.67    5.13    1.89    2.48    5.00
2.00     5.13    5.36    4.99    2.80    1.51    2.48    5.37    6.74    6.16
3.00     3.62    3.16    3.04    5.30    5.66    4.53    3.08    3.27    5.55
4.00     4.47    5.13    5.21    4.23    4.36    5.75    5.48    4.84    3.34
5.00     4.96    4.37    4.96    5.27    5.38    4.26    5.30    4.05    4.27
        NOZZLE EXIT
        1       3.42
        2       4.81
        3       3.68

                                     PORTS 1 THROUGH 9
        ROW             MEASURED TOTAL PRESSURE IN PSIA

1.00    20.06   21.78   20.07   29.04   40.31   35.62   18.27   21.74   28.04
2.00    26.56   30.65   29.50   20.97   15.83   23.08   33.32   35.35   35.50
3.00    19.77   26.36   22.67   34.11   23.58   27.15   22.02   26.40   29.67
4.00    21.41   30.08   28.91   24.68   19.75   26.45   27.20   32.59   21.37
5.00    23.48   28.13   27.15   25.80   21.81   25.73   23.90   28.03   22.74
        NOZZLE EXIT
        1     32.51
        2     40.49
        3     22.04

                                     PORTS 1 THROUGH 9
        ROW               ACTUAL TOTAL PRESSURE IN PSIA

1.00    23.36   48.75   37.07   58.79   53.28   58.39   42.03   44.82   38.72
2.00    34.78   42.95   42.38   36.87   40.17   51.02   49.68   46.65   50.05
3.00    26.82   51.66   39.71   52.37   27.37   39.39   37.03   49.98   39.68
4.00    26.73   42.94   39.62   35.11   23.90   32.28   34.69   51.95   32.62
5.00    29.11   43.18   36.89   32.64   25.01   37.55   28.85   45.76   30.33
        NOZZLE EXIT
        1     73.47
        2     80.08
        3     31.97

                                     PORTS 1 THROUGH 9
        ROW                              MACH NUMBER

1.00     1.69    2.64    2.40    2.51    1.92    2.24    2.67    2.54    1.99
2.00     1.91    2.02    2.05    2.33    2.79    2.62    2.11    1.92    2.02
3.00     1.97    2.47    2.33    2.15    1.69    2.07    2.27    2.43    1.94
4.00     1.83    2.04    1.98    2.04    1.77    1.78    1.86    2.20    2.14
5.00     1.81    2.15    1.97    1.85    1.66    2.08    1.76    2.23    1.94
        NOZZLE EXIT
        1      2.65
        2      2.48
        3      2.07
```

VITA

Major John M. Traxler was born on 20 March 1953 in Coral Gables, Florida. He graduated from high school in Walled Lake, Michigan in 1971. He was commissioned as a Second Lieutenant upon graduation from the United States Air Force Academy on 4 June 1975, with a Bachelor of Science in Astronautical Engineering. He completed navigator and electronic warfare training at Mather Air Force Base, California in 1977. He has served as both a Weapons Systems Officer in the F-4 and Electronic Warfare Officer in the F-4G, Wild Weasel with tours in Germany and George AFB, California. He attended Bible school in California and was ordained as a minister of the gospel of Jesus Christ, at whose pleasure he is privileged to serve. He entered the School of Engineering, Air Force Institute of Technology, in May 1986. Upon graduation he is assigned to the Spacecraft Divison, 6555 Aerospace Test Group, Cape Canaveral, Florida.

Permanent Address: 8400 Cascade
Union Lake, Michigan 48085

UNCLASSIFIED
SECURITY CLASSIFICATION OF THIS PAGE

AD-A189 572

REPORT DOCUMENTATION PAGE

Form Approved
OMB No. 0704-0188

1a. REPORT SECURITY CLASSIFICATION UNCLASSIFIED	1b. RESTRICTIVE MARKINGS
2a. SECURITY CLASSIFICATION AUTHORITY	3. DISTRIBUTION/AVAILABILITY OF REPORT Approved for public release; distribution unlimited.
2b. DECLASSIFICATION/DOWNGRADING SCHEDULE	
4. PERFORMING ORGANIZATION REPORT NUMBER(S) AFIT/GA/AA/87-07	5. MONITORING ORGANIZATION REPORT NUMBER(S)

6a. NAME OF PERFORMING ORGANIZATION	6b. OFFICE SYMBOL *(If applicable)*	7a. NAME OF MONITORING ORGANIZATION
6c. ADDRESS *(City, State, and ZIP Code)* Air Force Institute of Technology (AU) Wright-Patterson AFB, OH 45433-6583		7b. ADDRESS *(City, State, and ZIP Code)*
8a. NAME OF FUNDING/SPONSORING ORGANIZATION AF Aero Propulsion Laboratory	8b. OFFICE SYMBOL *(If applicable)* AFWAL/PS	9. PROCUREMENT INSTRUMENT IDENTIFICATION NUMBER

8c. ADDRESS *(City, State, and ZIP Code)*
Wright-Patterson AFB, OH 45433

10. SOURCE OF FUNDING NUMBERS

PROGRAM ELEMENT NO.	PROJECT NO.	TASK NO.	WORK UNIT ACCESSION NO.

11. TITLE *(Include Security Classification)*
See Block 19

12. PERSONAL AUTHOR(S)
John M. Traxler, Major, USAF

13a. TYPE OF REPORT	13b. TIME COVERED	14. DATE OF REPORT *(Year, Month, Day)*	15. PAGE COUNT
MS Thesis	FROM ______ TO ______	1987 December	112

16. SUPPLEMENTARY NOTATION

17. COSATI CODES

FIELD	GROUP	SUB-GROUP
20	04	
21	02	

18. SUBJECT TERMS *(Continue on reverse if necessary and identify by block number)*
Supersonic Combustion, Base Flow, Shock Waves
Two Dimensional Flow, Supersonic Nozzles

19. ABSTRACT *(Continue on reverse if necessary and identify by block number)*

Title: INTERACTION BETWEEN TWO-DIMENSIONAL SONIC JETS AND SUPERSONIC FLOW TO MODEL HEAT ADDITION IN A SUPERSONIC COMBUSTOR

Thesis Chairman: Dr. William C. Elrod
Professor of Aerospace Engineering

Approved for public release: IAW AFR 190-1.
Lynn Wolaver
LYNN E. WOLAVER 31 Dec 87
Dean for Research and Professional Development
Air Force Institute of Technology (AFC)
Wright-Patterson AFB OH 45433

20. DISTRIBUTION/AVAILABILITY OF ABSTRACT ☒ UNCLASSIFIED/UNLIMITED ☐ SAME AS RPT. ☐ DTIC USERS	21. ABSTRACT SECURITY CLASSIFICATION UNCLASSIFIED

22a. NAME OF RESPONSIBLE INDIVIDUAL	22b. TELEPHONE *(Include Area Code)*	22c. OFFICE SYMBOL
Dr. William C. Elrod	513-255-3517	AFIT/ENG

DD Form 1473, JUN 86 *Previous editions are obsolete.* SECURITY CLASSIFICATION OF THIS PAGE

In this investigation the displacement effects of heat addition to a supersonic flow through a simulated combustor were simulated with mass addition. The structure of precombustion shocks was experimentally investigated by an optical and pressure study of two parallel sonic jets expanding into a two-dimensional supersonic test cavity. Base flow and recompression shocks were studied for two test section depths. A test section to add heat to a two dimensional flow was demonstrated.

It was determined that the performance of the constant-area test section was dominated by frictional, rather than shock effects. An off-design nozzle ~~was~~ used for preliminary investigation, ~~and~~ caused turbulence and high losses in the channel. The structure of the precombustion zone was found to be a base flow problem and was analyzed using a simple one dimensional model. Static pressure measurements on the sidewalls of the test cavity were found to differ from the static pressure in the center of the two dimensional test cavity, due to diffusion of pressure upstream and downstream through the boundary layer.

A welding torch was used to inject premixed oxygen and acetylene into the base region on the end of a centerbody between two supersonic nozzles. The flame was sucessfully ignited and burned continuously in the flowstream. However, the large amount of heat added caused flow separation in the supersonic nozzles.

END

DATE

3-88

DTIC